

RESEARCH ARTICLE

Mouse myofibers lacking the SMYD1 methyltransferase are susceptible to atrophy, internalization of nuclei and myofibrillar disarray

M. David Stewart^{1,*}, Suhujey Lopez¹, Harika Nagandla¹, Benjamin Soibam², Ashley Benham³, Jasmine Nguyen¹, Nicolas Valenzuela¹, Harry J. Wu¹, Alan R. Burns⁴, Tara L. Rasmussen⁵, Haley O. Tucker^{6,‡} and Robert J. Schwartz^{1,3}

ABSTRACT

The *Smyd1* gene encodes a lysine methyltransferase specifically expressed in striated muscle. Because *Smyd1*-null mouse embryos die from heart malformation prior to formation of skeletal muscle, we developed a *Smyd1* conditional-knockout allele to determine the consequence of SMYD1 loss in mammalian skeletal muscle. Ablation of SMYD1 specifically in skeletal myocytes after myofiber differentiation using *Myf6^{Cre}* produced a non-degenerative myopathy. Mutant mice exhibited weakness, myofiber hypotrophy, prevalence of oxidative myofibers, reduction in triad numbers, regional myofibrillar disorganization/breakdown and a high percentage of myofibers with centralized nuclei. Notably, we found broad upregulation of muscle development genes in the absence of regenerating or degenerating myofibers. These data suggest that the afflicted fibers are in a continual state of repair in an attempt to restore damaged myofibrils. Disease severity was greater for males than females. Despite equivalent expression in all fiber types, loss of SMYD1 primarily affected fast-twitch muscle, illustrating fiber-type-specific functions for SMYD1. This work illustrates a crucial role for SMYD1 in skeletal muscle physiology and myofibril integrity.

KEY WORDS: Genetics, Development, Muscle, Myocyte, SMYD1, Methylation, Myopathy

INTRODUCTION

The *SMYD1* gene encodes an evolutionarily conserved histone methyltransferase containing a catalytic SET domain split by a zinc-finger-rich MYND domain. The SET domain is required for trimethylation of histone H3 lysine 4 (H3K4me3) (Sirinupong et al., 2010; Tan et al., 2006), a chromatin modification associated with active transcription (Strahl et al., 1999). The MYND domain is a protein-protein interaction motif best known for its association with histone deacetylase (HDAC)-containing co-repressor complexes (Liu et al., 2007; Lutterbach et al., 1998; Masselink and Bernards, 2000).

Thus, SMYD1 possesses both transcriptional activator and repressor properties. SMYD1 also localizes to the sarcoplasm, where it directly interacts with myosin through its C-terminal region (Just et al., 2011).

Expression of *SMYD1* is highly restricted to the striated muscles of human, fish, frog, chicken and mouse (Gottlieb et al., 2002; Kawamura et al., 2008; Li et al., 2009; Tan et al., 2006). *Smyd1* mRNA was detected in the earliest cardiac progenitor cells within the precardiac mesoderm. Later in embryonic development, its expression becomes restricted to the myocardium (Gottlieb et al., 2002; Rasmussen et al., 2015). In the skeletal muscle lineage, *Smyd1* mRNA is detectable within the somites as early as embryonic day 9.5 (E9.5); protein is first detectable within differentiating myoblasts (Nagandla et al., 2016). Expression persists in both cardiac and skeletal myocytes throughout development and into adulthood.

SMYD1 plays an essential role in heart and skeletal muscle development. *Smyd1*-null mice die *in utero* prior to skeletal muscle development, owing to heart defects (Gottlieb et al., 2002). Because of this early lethality, information regarding the *in vivo* skeletal muscle function(s) of SMYD1 has been limited to studies in zebrafish. Zebrafish have two highly similar genes, *smyd1a* and *smyd1b*. Knockdown of *smyd1b* results in disruption of myofibril formation in both skeletal and cardiac muscles (Li et al., 2013; Tan et al., 2006). Likewise, the zebrafish mutant *flatline (fla)*, carrying a null mutation within *smyd1b*, fails to form sarcomeres (Just et al., 2011). Individual morpholino knockdowns of the two *smyd1* genes showed *smyd1b* to be more crucial of the two for myofibrillogenesis; however, ectopic expression of *smyd1a* can substitute for loss of *smyd1b* (Gao et al., 2014). The mammalian and zebrafish *Smyd1* genes encode two mRNA transcripts via inclusion or exclusion of a small exon encoding 13 amino acids (Hwang and Gottlieb, 1997). Although differential functions for these isoforms have not been addressed in mouse or human, the zebrafish protein encoded by the inclusion of the small exon localizes to the M-line, whereas the shorter isoform exhibits weak sarcomere association (Li et al., 2011). The precise function of SMYD1 in myofibrillogenesis has remained unclear regardless of species. SMYD1 associates with nascent myosin during sarcomerogenesis and then localizes to the M-line of mature sarcomeres (Just et al., 2011). Thick filament chaperones are upregulated in the absence of *smyd1b*, supporting the idea that SMYD1 stabilizes myosin (Li et al., 2013). Collectively, the published data concur that SMYD1 is a striated-muscle-specific methyltransferase essential for proper development of cardiac and skeletal muscle, and which might stabilize assembly of the contractile apparatus. Thus, further investigation of the molecular biology of SMYD1 is essential to our understanding of the molecular genetics of muscle physiology.

To circumvent embryonic lethality in mice, we generated a *Smyd1* conditional-knockout (CKO) allele (Rasmussen et al., 2015) to test the hypothesis that SMYD1 is required for proper skeletal

¹Department of Biology and Biochemistry, University of Houston, Houston, TX 77204, USA. ²Department of Computer Science and Engineering Technology, University of Houston-Downtown, Houston, TX 77002, USA. ³Stem Cell Engineering Department, Texas Heart Institute at St Luke's Episcopal Hospital, Houston, TX 77030, USA. ⁴College of Optometry, University of Houston, Houston, TX 77204, USA. ⁵Department of Molecular Physiology, Baylor College of Medicine, Houston, TX 77030, USA. ⁶Department of Molecular Biosciences, Institute for Cellular Molecular Biology, The University of Texas at Austin, Austin, TX 78712, USA. [‡]Contact for mouse strain requests (haley.tucker@austin.utexas.edu)

*Author for correspondence (dstewart@uh.edu)

This is an Open Access article distributed under the terms of the Creative Commons Attribution License (<http://creativecommons.org/licenses/by/3.0>), which permits unrestricted use, distribution and reproduction in any medium provided that the original work is properly attributed.

muscle development in mammals. Specific inactivation of *Smyd1* in skeletal myocytes resulted in a myopathy with excessive internal nuclei, atrophy and myofibril disarray. The pathology was primarily manifest in fast-twitch muscles, with males being more severely affected than females. These phenotypic findings along with gene-expression profiling suggest a mechanism by which myofibers fail to fully mature. That SMYD1 also regulates cardiac development and function opens the possibility that *SMYD1* is a genetic link between skeletal and cardiac myopathies.

RESULTS

To determine the function of SMYD1 in skeletal muscle, we conditionally inactivated the *Smyd1* gene using *Myf6^{cre}*. In this strain, an internal ribosome entry site (*IRES*)-*Cre* cassette is located within the 3' untranslated region (UTR) of the *Myf6* gene, allowing bicistronic expression of *Myf6* and *Cre* (Keller et al., 2004). Our genetic approach included the *Rosa26^{YFP}* allele, which allowed us to monitor cells derived from *Myf6^{cre}*-expressing cells. By monitoring yellow fluorescent protein (YFP) fluorescence, we found the onset of *Myf6^{cre}*-induced recombination to occur at E17.5, being just barely detectable in skeletal muscles at this point. Strong YFP fluorescence was not observed until the day of birth (data not shown). *Smyd1* is first expressed in the somitic myoblasts as early as E9.5 and expression persists throughout myogenesis and in mature myofibers (Gottlieb et al., 2002; Nagandla et al., 2016). Thus, SMYD1 might have roles in both myogenesis and myofiber homeostasis. Using *Myf6^{cre}*, we specifically studied the role of SMYD1 in myofibers post-myogenesis. Using 6-week-old mice, we confirmed that *Myf6^{cre}* induces recombination of *loxP* sites in all muscles examined (Fig. S1). All experiments were performed and tissues collected at 6 weeks of age unless otherwise noted.

Smyd1 CKO mice are smaller with reduced strength

Western blots were performed to confirm loss of SMYD1 protein in CKO muscles. SMYD1 protein levels were undetectable in both the tibialis anterior and soleus of CKO mice (Fig. 1A). Visually, male CKOs appeared smaller than control littermates. Female CKOs appeared only marginally smaller than control littermates (Fig. 1B,C). Body weight was reduced for both male and female CKO mice compared with controls (Fig. 1D). Males, but not females, exhibited reduced body length (naso-anal length) (Fig. 1E).

Suspecting some form of myopathy in *Smyd1* CKO mice, we performed several experiments to assay strength. A four-paw grip strength test revealed weakness for both CKO males and females (Fig. 1F). We assayed relative strength/endurance with an inverted grid hanging test, which measures the length of time that the mouse can cling upside down before falling. Male CKOs underperformed controls in this test. In contrast, female CKOs performed equal to controls (Fig. 1G). Last, we performed accelerating rotarod tests, which assay strength, motor coordination and learning (males, Fig. 1H; females, Fig. 1I). With successive trials, mice of all groups progressively increased the length of time they could run on the rotarod. Male and female CKOs underperformed their control counterparts; however, the mean difference in elapsed time for male controls vs male CKOs (55.1±7.7 s) was much greater than that for female controls vs female CKOs (17.8±7.9 s). Collectively, these results revealed loss of strength and reduced endurance in the absence of SMYD1, which more severely affected male mice.

Smyd1 CKO mice exhibited reduced muscle mass

Body composition was assayed by magnetic resonance imaging (MRI) and showed reduced lean mass and increased fat mass for both

CKO males and females compared with sex-matched controls (Fig. 2A,B). Individual muscles, comprising a range of fiber-type compositions (tibialis anterior, fast twitch; soleus, slow twitch; gastrocnemius and triceps, mixed), were dissected and weighed. In males, we observed reduced mass for all muscles studied. For females, a significant difference in mass was observed for gastrocnemius, triceps and tibialis anterior, but not soleus (Fig. 2C-F). At the gross morphological level, *Smyd1* CKO muscles appeared smaller than those of control mice (males, Fig. 2G; females, Fig. S2).

High percentage of fibers with central nuclei in fast-twitch muscle

We next examined the consequence of *Smyd1* deficiency on the histology of a number of muscles/muscle groups (triceps, quadriceps, gastrocnemius, tibialis anterior and soleus) in hematoxylin and eosin (H&E)-stained sections. Representative images from male and female tibialis anterior and soleus are shown in Fig. 3A-D,I-L and for triceps, quadriceps and gastrocnemius in Fig. S3. Although no necrotic or degenerating fibers were apparent, we observed a large number of fibers with central/internal nuclei and hypotrophic fibers. Quantification of the percentage of fibers with central nuclei in the tibialis anterior (fast twitch) and soleus (slow twitch) at 6 weeks of age revealed that, in male mice, 19% of fibers in the *Smyd1* CKO tibialis anterior exhibited central nuclei as compared to 0.8% of fibers in controls (Fig. 3E). Compared to controls, female *Smyd1* CKOs also exhibited increased numbers of fibers with central nuclei in the tibialis anterior (9% in CKOs vs 0.8% in controls) (Fig. 3M). Note that the percentage of fibers with central nuclei in female CKOs was less than that for male CKOs (males, 19%; females, 9%).

Myofiber size was quantified by measuring minimum Feret diameter. The tibialis anterior of *Smyd1* CKO male mice exhibited increased numbers of hypotrophic fibers as compared to control littermates (mean min. Feret diameter: Ctrl, 31.18±0.80 μm; CKO, 25.15±0.83 μm; ANOVA, *P*<0.05) (Fig. 3F). Female *Smyd1* CKO mice also exhibited myofiber hypotrophy in the tibialis anterior (mean min. Feret diameter: Ctrl, 29.70±1.34 μm; CKO, 26.44±1.71 μm; ANOVA, *P*<0.05) (Fig. 3N). Consistent with our strength, muscle mass and central nuclei data, the percent reduction in fiber size was less for *Smyd1* CKO females than for males (19% for males vs 11% for females). In neither males nor females was the soleus significantly affected by this myopathy as judged by % central nuclei (Fig. 3G,O) or minimum Feret diameter (mean min. Feret diameter: Ctrl males, 25.72±1.05 μm; CKO males, 26.45±0.65 μm; Ctrl females, 29.70±1.34 μm; CKO females, 26.44±1.71 μm; ANOVA, *P*>0.05) (Fig. 3H,P). Thus, the major pathological features primarily affect fast-twitch muscle. Furthermore, these data indicate a gender-specific effect in which males are more severely affected than females. Because males displayed a consistent strong phenotype, the remainder of the experiments were conducted using only male tissues.

To determine whether disease worsened with age, we allowed a group of male mice to age to 6 months. Disease progression was little changed for the tibialis anterior but increased in the soleus. We observed high numbers of hypotrophic fibers and fibers with central nuclei in the tibialis anterior (Fig. S4A,B). In contrast to younger (6-week-old) CKOs, the soleus now showed increased numbers of fibers with central nuclei (Fig. S4C,D). For the tibialis anterior, the percentage of fibers with centralized nuclei was 21% (Fig. S4E), similar to that observed at 6 weeks. Unlike 6-week-old mice, *Smyd1* CKO soleus exhibited significantly more fibers with central nuclei than controls, albeit a modest increase. *Smyd1* CKO soleus exhibited

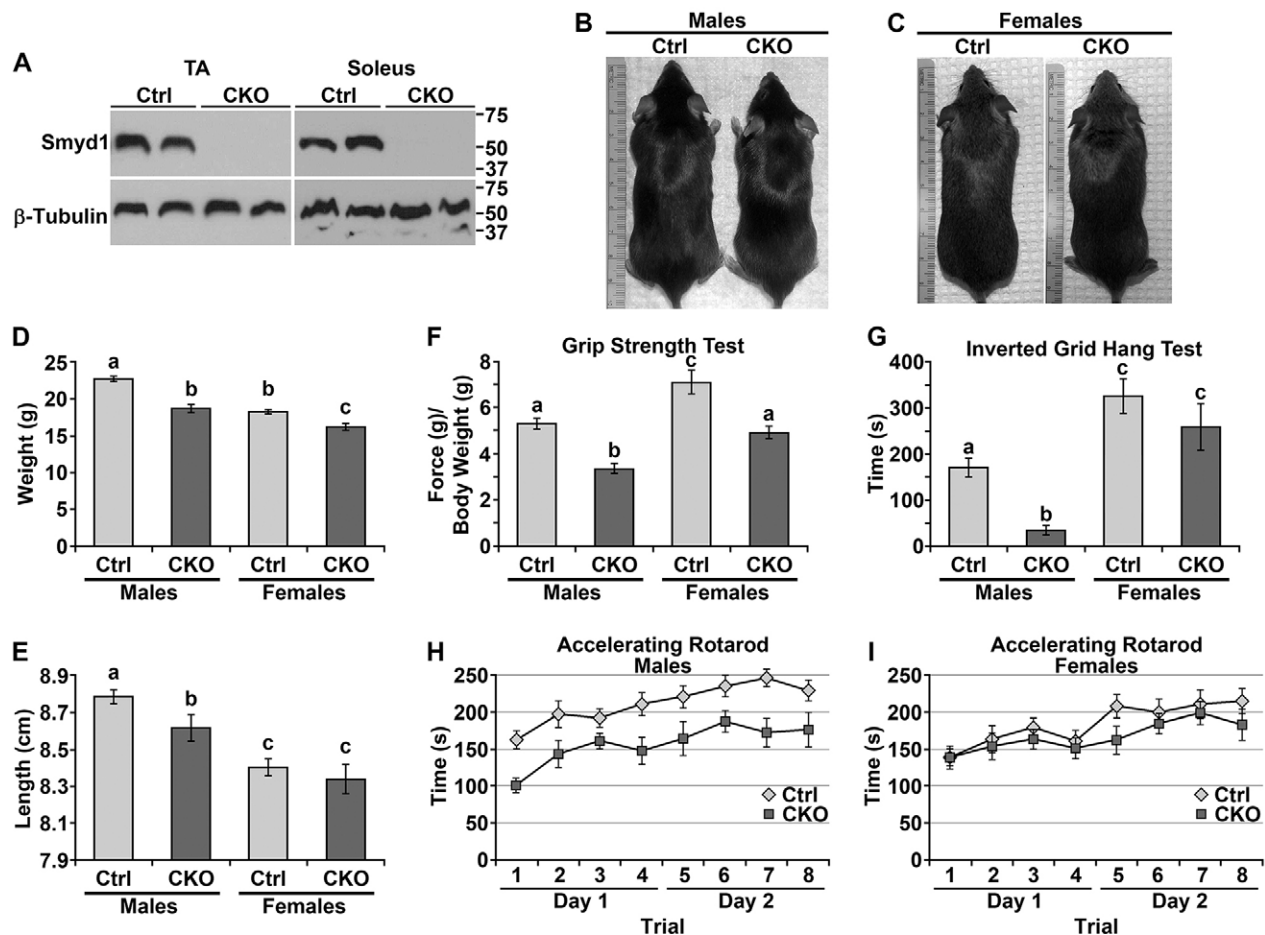


Fig. 1. *Smyd1* CKO mice are smaller with reduced strength. (A) Western blots showing the absence of SMYD1 protein in CKO muscles. (B,C) *Smyd1* CKO males appeared slightly smaller than controls. Female CKOs appeared similar to controls. (D) *Smyd1* CKO mice weighed less than controls. $n \geq 17$ animals/group. (E) Body length (naso-anal length) was reduced for *Smyd1* CKO males, but not females. $n \geq 17$ animals/group. (F,G) *Smyd1* CKO mice were weaker than controls. (F) Four-paw grip-strength tests. Data are maximum force of three pulls per animal normalized to body weight. $n \geq 8$ animals/group. (G) Inverted grid hang tests. Data are the length of time the mouse is able to hang from the grid before falling. $n \geq 13$ animals/group. (D-G) Statistics were ANOVA+post hoc tests. Significant differences ($P < 0.05$) are denoted by the lowercase letters above each bar. (H,I) Accelerating rotarod tests for males (H) and females (I). Mice of all groups progressively increased the length of time they could run on the rotarod (two-way ANOVA, $P < 0.001$ for both males and females). Male and female CKOs underperformed their control counterparts (two-way ANOVA; males: $P < 0.0001$, $n \geq 12$ animals/group; females: $P = 0.025$, $n \geq 13$ animals/group); however, the mean difference in elapsed time for male controls vs male CKOs (55.1 ± 7.7 s) was much greater than that for female controls vs female CKOs (17.8 ± 7.9 s). All data was obtained at 6 weeks of age. Error bars show s.e.m. Ctrl, control; CKO, conditional knockout; TA, tibialis anterior.

4% of fibers with central nuclei, whereas controls exhibited less than 1% (Fig. S4G). For tibialis anterior, average fiber minimum Feret diameter for control mice increased with age to $41.32 \pm 1.64 \mu\text{m}$, as compared to $30.96 \pm 0.54 \mu\text{m}$ for CKO mice – a value similar to that observed for CKOs at 6 weeks (ANOVA, $P < 0.05$) (Fig. S4F). For the soleus we observed no significant difference in fiber size distribution (mean min. Feret diameter: Ctrl, $32.55 \pm 0.79 \mu\text{m}$; CKO $31.04 \pm 0.72 \mu\text{m}$; ANOVA, $P > 0.05$) (Fig. S4H).

Absence of regenerating myofibers and normal sarcolemma in *Smyd1* CKO muscle

To determine whether the myofibers with central nuclei were the result of regeneration, we assayed the number of regenerating fibers by immunolocalization of embryonic myosin heavy chain (eMyHC). The tibialis anterior of control mice exhibited no eMyHC-positive fibers (Fig. 4A). Only a single small eMyHC positive fiber was found in the three CKOs assayed (Fig. 4B). Thus, eMyHC-marked regenerating fibers do not correlate with the presence of central nuclei. Furthermore, the extremely low numbers of regenerating

fibers cannot account for the 20% of fibers with central nuclei. Newborn (postnatal day 0) hindlimb, which is rich in eMyHC-positive fibers, was used as a positive control (Fig. 4C). We next assayed a representative panel of regeneration genes for alterations in transcript expression. Expression of *Pax3* and *Myod1* was unaffected (Fig. 4D,F), whereas expression of *Pax7* and *Myog* was modestly increased (Fig. 4E,G).

Sarcolemmal integrity in the tibialis anterior was assayed by Evans blue dye uptake. No Evans-blue-dye-positive fibers were identifiable in control or *Smyd1* CKO mice that were unexercised (Fig. 4H,I) or subjected to a single period of treadmill exercise (30 min at 12 m/min, uphill 5°) (Fig. 4K,L). As a positive control, we observed widespread Evans-blue-dye-positive fibers in control mice that received a single intramuscular injection of cardiotoxin 13 days earlier (Fig. 4J,M). Thus, sarcolemmal integrity is intact in *Smyd1* CKO myofibers, which is indicative of myopathy rather than muscular dystrophy.

Collectively, these data indicate very low levels of regeneration, and normal sarcolemmal integrity, in the absence of SMYD1. These

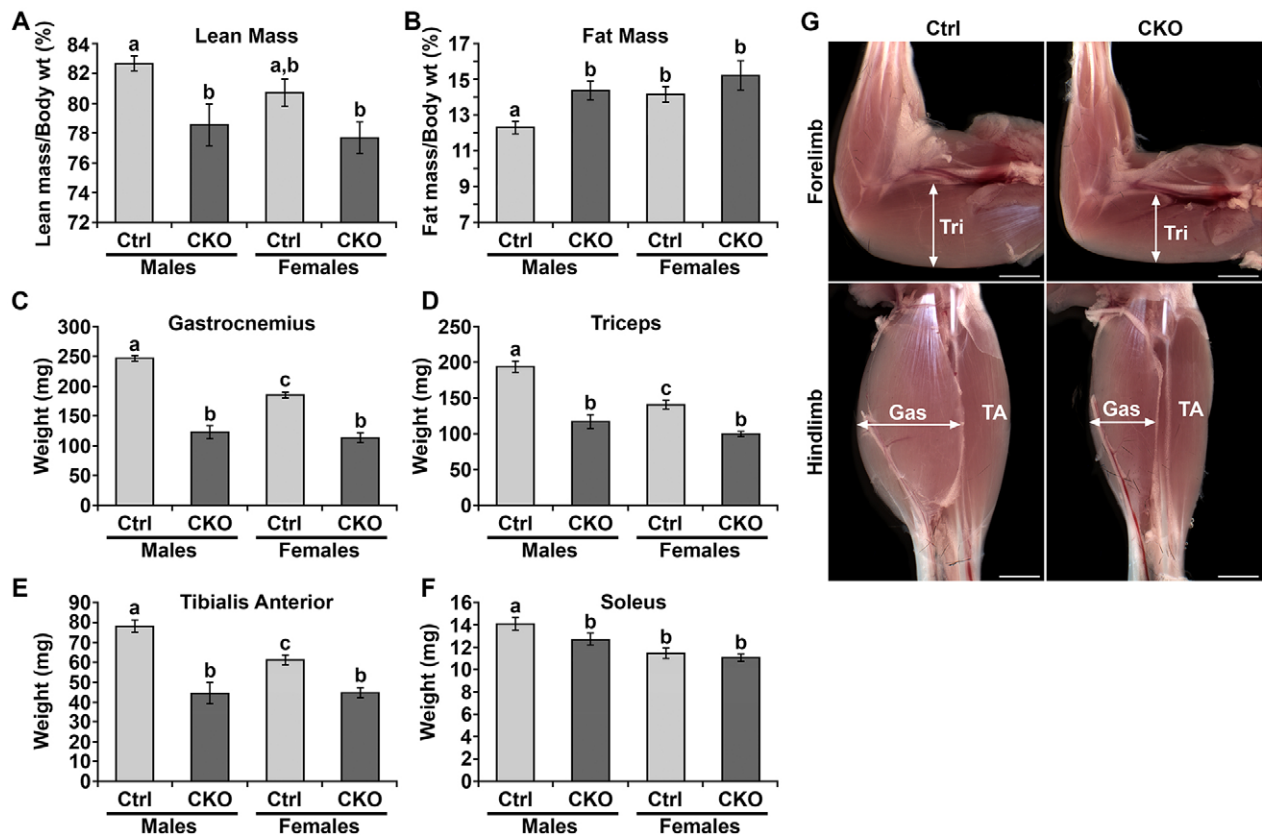


Fig. 2. *Smyd1* CKO mice exhibited reduced muscle mass. (A,B) Body composition analysis by MRI ($n \geq 12$ animals/group). (A) Percent lean mass was reduced in *Smyd1* CKO males and females. (B) Percent fat mass was increased in *Smyd1* CKO males and females. (C-F) Wet weight of individual muscles (weighed in pairs). For males, muscle mass was reduced for all muscles examined. For females, muscle mass was reduced for all except the soleus ($n \geq 10$ animals/group for gastrocnemius, soleus and triceps; $n \geq 6$ animals/group for tibialis anterior). (G) Stereoimages of the muscles of the forelimbs and hindlimbs (males only). Scale bars: 2 mm. All data was obtained at 6 weeks of age. Statistics were ANOVA+post hoc tests. Significant differences ($P < 0.05$) are denoted by the lowercase letters above each bar. Error bars show s.e.m. Ctrl, control; CKO, conditional knockout; Gas, gastrocnemius; TA, tibialis anterior; Tri, triceps.

minor increases in regeneration markers cannot account for the large numbers of fibers with central nuclei. These data coupled with the absence of necrotic or degenerating fibers suggest that the myofibers with internal nuclei have failed to fully mature rather than being the result of *de novo* regeneration.

Increased numbers of oxidative myofibers

The prevalence of internal myonuclei in the absence of regenerating fibers is reminiscent of human centronuclear myopathy (CNM). CNM is typically associated with type I fiber predominance and, in the case of *DNM2*- and *BIN1*-related CNM, a radial intermyofibrillar network (Böhm et al., 2014; Chen et al., 2015; Cowling et al., 2014; Romero, 2010; Romero and Bitoun, 2011). To study these characteristics, we performed NADH-tetrazolium reductase (NADH-TR) staining on frozen sections of tibialis anterior. We observed increased prevalence of oxidative fibers in the *Smyd1* CKO (Fig. 5A-D). At high magnification, we found no evidence for radial orientation of the intermyofibrillar network. The only irregularity observed was a central dense focus of oxidative stain (Fig. 5E,F). These dense foci generally, but not always, correlated with centralized nuclei (Fig. 5G). Centralized nuclei were observed in glycolytic, intermediate and oxidative fibers (Fig. 5H-J); however, they were most abundant in glycolytic fibers (Fig. 5K).

Abundance of type I fibers was assayed by immunofluorescence. We found no significant difference in the percentage of type I fibers in the tibialis anterior for controls and *Smyd1* CKOs (Ctrl, $0.51 \pm 0.89\%$;

CKO, $3.83 \pm 5.18\%$; $n = 7$ /group) (Fig. 5L,M). Soleus served as a positive control (Fig. 5N). These results were confirmed by the virtually undetectable levels of slow MyHC in tibialis anterior western blots (Fig. 5O). Interestingly, total MyHC levels were increased in *Smyd1* CKOs. Collectively, these data suggest increased fast-oxidative fiber abundance in the absence of SMYD1, but very little fast-to-slow fiber-type switching.

Abnormal myofibrillar architecture in the absence of SMYD1

The most notable ultrastructure abnormality was regional disorganization of myofibrils. Ultrastructure was assayed by transmission electron microscopy (TEM) using sections from the tibialis anterior. Control mice exhibited uniform evenly spaced parallel sarcomeres (Fig. 6A,D). *Smyd1* CKO tibialis anterior exhibited many regions where myofibrillar architecture appeared normal (Fig. 6B); however, regions of antiparallel sarcomeres (Fig. 6C) or general disorganization (Fig. 6E) were not uncommon. Foci of complete sarcomere disassembly were also found (Fig. 6F). Because these foci are visible in Toluidine-blue-stained sections under the light microscope, we were able to measure their area and abundance. The foci ranged in size from 30.4 to $1062.7 \mu\text{m}^2$ and covered $2.4 \pm 1.1\%$ of total longitudinal area. The average size of a single focus was $271.5 \pm 29.2 \mu\text{m}^2$. Data were derived from 96 measurements from three animals (>27 measurements/animal). Actin/myosin hexagons appeared normal in all transverse sections (Fig. 6J,K).

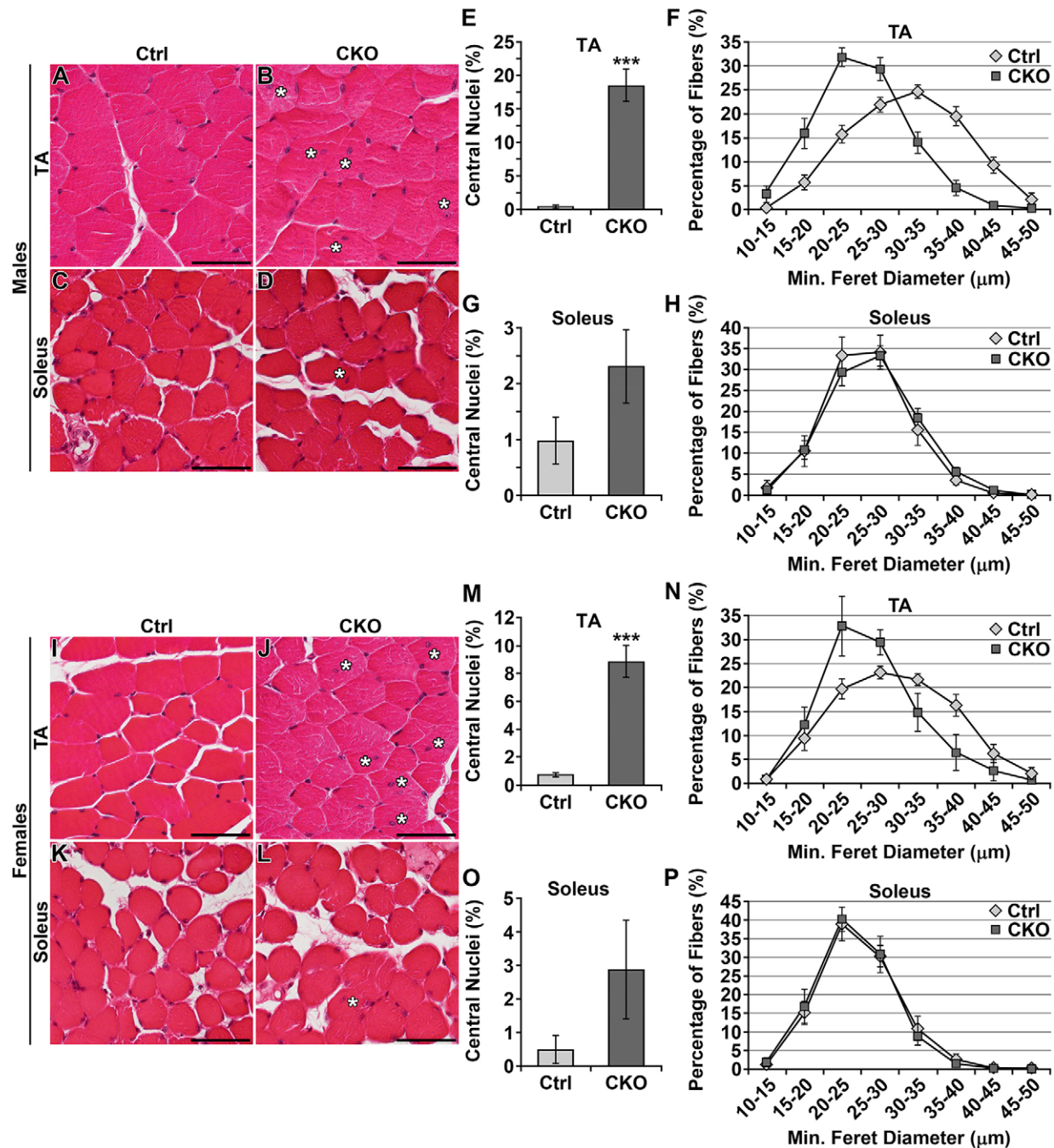


Fig. 3. High percentage of fibers with central nuclei in fast-twitch muscle. (A-H) 6-week-old males. (A-D) Central nuclei were prevalent in the *Smyd1* CKO tibialis anterior. White asterisks (*) indicate central nuclei. (E) Percentage of tibialis anterior myofibers with central nuclei ($n \geq 6$ animals/group). (F) Distribution of myofiber minimum Feret diameter in the tibialis anterior. *Smyd1* CKO tibialis anterior had increased numbers of hypotrophic fibers (ANOVA, $P < 0.05$; $n \geq 6$ animals/group). (G) Percentage of myofibers with central nuclei in the soleus. The difference was not significant ($n \geq 7$ animals/group). (H) Distribution of myofiber minimum Feret diameter in the soleus. No difference was observed ($n \geq 7$ animals/group). (I-P) 6-week-old females. (I-L) Central nuclei were prevalent in the CKO tibialis anterior, but to a lesser extent than observed for CKO males. (M) Percentage of tibialis anterior myofibers with central nuclei ($n = 6$ animals/group). (N) Distribution of myofiber minimum Feret diameter in the tibialis anterior. *Smyd1* CKO tibialis anterior had increased numbers of hypotrophic fibers (ANOVA, $P < 0.05$; $n = 6$ animals/group). (O) Percentage of myofibers in the soleus with central nuclei. The difference was not significant ($n \geq 10$ animals/group). (P) Distribution of myofiber minimum Feret diameter in the soleus. No difference was observed ($n \geq 10$ animals/group). *** $P < 0.001$, Student's *t*-test. Error bars show s.e.m. Scale bars: 50 μm . Ctrl, control; CKO, conditional knockout; TA, tibialis anterior.

Human CNM is linked to impaired excitation-contraction coupling as a result of irregular triad structure or reduced numbers of triads (Jungbluth and Gautel, 2014; Romero and Bitoun, 2011). Control mice exhibited vast numbers of triads with correct appearance (Fig. 6G). In *Smyd1* CKO muscle, no obvious

abnormalities were noted in triad structure regardless of whether the triad was located in a region with normal myofibrillar architecture (Fig. 6H) or a region of disorganized myofibrils (Fig. 6I). However, *Smyd1* CKO mice exhibited reduced numbers of triads as measured by counting the number of triads that flanked

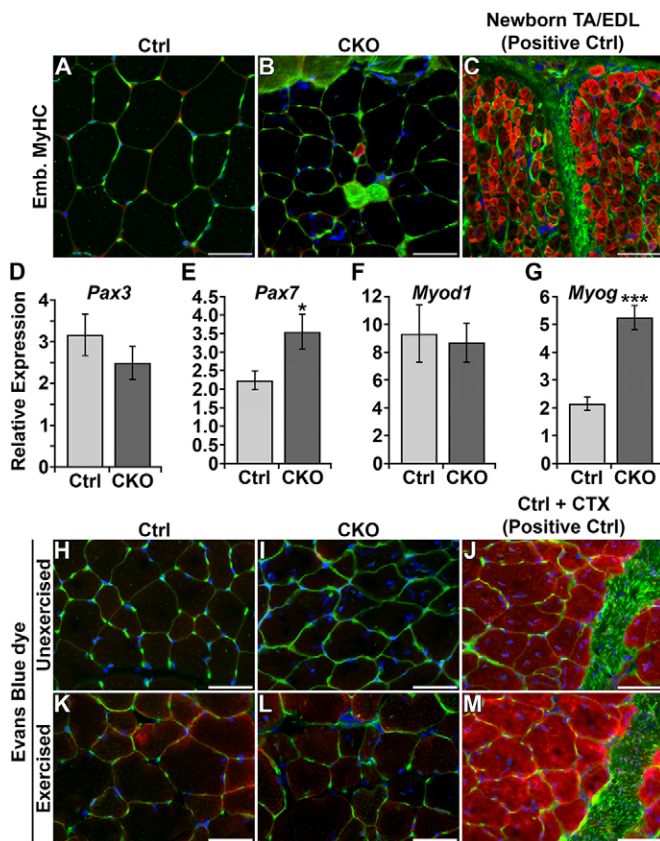


Fig. 4. Absence of regenerating myofibers and normal sarcolemma in *Smyd1* CKO muscle. (A-C) Near complete lack of embryonic myosin heavy chain (eMyHC)-positive myofibers in the *Smyd1* CKO. Red, eMyHC; green, sarcolemma (WGA-488); blue, nuclei (DAPI). No eMyHC-positive myofibers were found in control animals ($n=3$) (A). Only a single eMyHC-positive myofiber was found in *Smyd1* CKO tibialis anterior ($n=3$) (B). Newborn (postnatal day 1) hindlimb muscles were used as a positive control for eMyHC (C). (D-G) Results of real-time PCR assays for regeneration-associated genes ($n=6$ animals/group). Expression of *Pax3* (D) and *Myod1* (F) were unchanged. Expression of *Pax7* (E) and *Myog* (G) were increased in the *Smyd1* CKO. (H-M) No evidence for impaired sarcolemmal integrity in the *Smyd1* CKO. Red, Evans blue dye; green, sarcolemma (WGA-488); blue, nuclei (DAPI). Uptake of Evans blue dye in unexercised (H,I) or exercised (K,L) mice ($n=3$ animals/group). Cardiotoxin-treated muscle was used as a positive control (J,M). All assays were performed using tibialis anterior muscle from 6-week-old male mice. * $P<0.05$, *** $P<0.001$, Student's *t*-test. Error bars show s.e.m. Scale bars: 50 μ m. Ctrl, control; CKO, conditional knockout; CTX, cardiotoxin; EDL, extensor digitorum longus; TA, tibialis anterior.

each Z-line. Normally, two triads flank each Z-line at the myofibril border. *Smyd1* CKO mice had fewer junctions with two triads and increased junctions with none or a single triad compared with controls (Fig. 6L). These data indicate intact triad structure but reduced complexity of the triad network in the absence of SMYD1.

Gene expression alterations were specific to fast-twitch muscle

Looking for a connection between SMYD1 and CNM-associated pathways, we quantified transcript levels for the six major genes linked to CNM by real-time PCR (Table 1). In the tibialis anterior, we found upregulation of *Ryr1* and downregulation of *Ptpla*. *Bin1*, *Dnm2*, *Mtm1* and *Mtmr14* were unchanged. None of these genes showed altered expression in the soleus.

Because we found total MyHC protein levels to be elevated in the CKO (Fig. 5O), we assayed mRNA levels for the major MyHC

isoforms (Table 1). Gene expression of all MyHC isoforms (*Myh1*, 2, 4, 7) was increased in the tibialis anterior, but not in the soleus. These data further support the notion that the myopathy primarily affects fast-twitch muscle.

Unlike what we observed in the mouse, zebrafish morpholino or natural *smyd1a/b* mutants exhibit very severely impaired sarcomerogenesis (Just et al., 2011; Li et al., 2013; Tan et al., 2006). Thus, we reasoned that other SMYD family members might compensate for the loss of *Smyd1* in mice. To this end, we assayed expression of *Smyd2*, 3, 4 and 5 (all known SMYD family members) (Table 1). We found *Smyd2* expression to be downregulated in the *Smyd1* CKO tibialis anterior. Expression of *Smyd3*, 4 and 5 was unaffected. No gene expression alterations were found in the soleus. Because no other SMYD family member was upregulated in response to the absence of SMYD1, it is unlikely that other SMYD family members compensate for the loss of SMYD1 in mice.

Our data consistently revealed a myopathy that primarily affected fast-twitch muscle. One explanation for this is that *Smyd1* might not be expressed in slow-twitch fibers, as was reported in zebrafish embryos (Just et al., 2011). Thus, we tested whether *Smyd1* is expressed in type I and II fibers by immunofluorescence using longitudinal sections of the extensor digitorum longus (EDL; which was used for ease of obtaining longitudinal sections) and soleus. Slow MyHC⁺ fibers were abundant in the soleus (Fig. S5A), but extremely rare in the EDL (Fig. S5B). SMYD1 showed sarcolemmal localization in all fibers of both muscles (Fig. S5C,D). Next, we compared *Smyd1* mRNA and protein levels in the tibialis anterior and soleus by real-time PCR and western blot, respectively. The tibialis anterior and soleus showed comparable levels of *Smyd1* mRNA (Fig. S5G). SMYD1 protein levels were slightly higher in the tibialis anterior compared to the soleus (Fig. S5H). Thus, in mice, *Smyd1* is expressed in all fiber types. Furthermore, no other SMYD family members are upregulated to compensate for the loss of *Smyd1* in the soleus (Table 1). These data indicate that, despite SMYD1's presence in all fiber types, its absence produces defects that primarily manifest within type II fibers.

Genes involved in muscle development are upregulated in *Smyd1* CKO muscle

To gain better insight into how loss of SMYD1 affected the myocyte transcriptome, we compared global gene expression in control versus *Smyd1* CKO tibialis anterior by RNA sequencing (RNA-seq). Expression of 603 genes was significantly upregulated (Fig. S6A) and expression of 630 genes was significantly downregulated (Fig. S6B) in the *Smyd1* CKO (cutoff was $P<0.05$). The top ten gene ontology terms associated with upregulated genes were primarily composed of muscle development pathways (Fig. S6C). Of the 42 genes upregulated in muscle gene ontology categories, 14 encode myofibrillar proteins and five encode regeneration-associated transcription factors. Also upregulated were ion channels, neuromuscular junction proteins, membrane structural components and signal transduction molecules. A heat map of upregulated genes associated with muscle gene ontology terms is presented in Fig. S7. The top ten gene ontology terms associated with downregulated genes mostly fell into the category of energy metabolism (Fig. S6D). Very few genes associated with fibrosis or inflammation exhibited altered expression in *Smyd1* CKO muscle, supporting the idea that this is not a degenerative muscle disease (Fig. S8). Because CNM is usually associated with impaired structure or function of the excitation-contraction coupling apparatus, we scrutinized the gene expression data for differentially expressed genes associated with T-tubules, membrane dynamics or calcium channels and found a

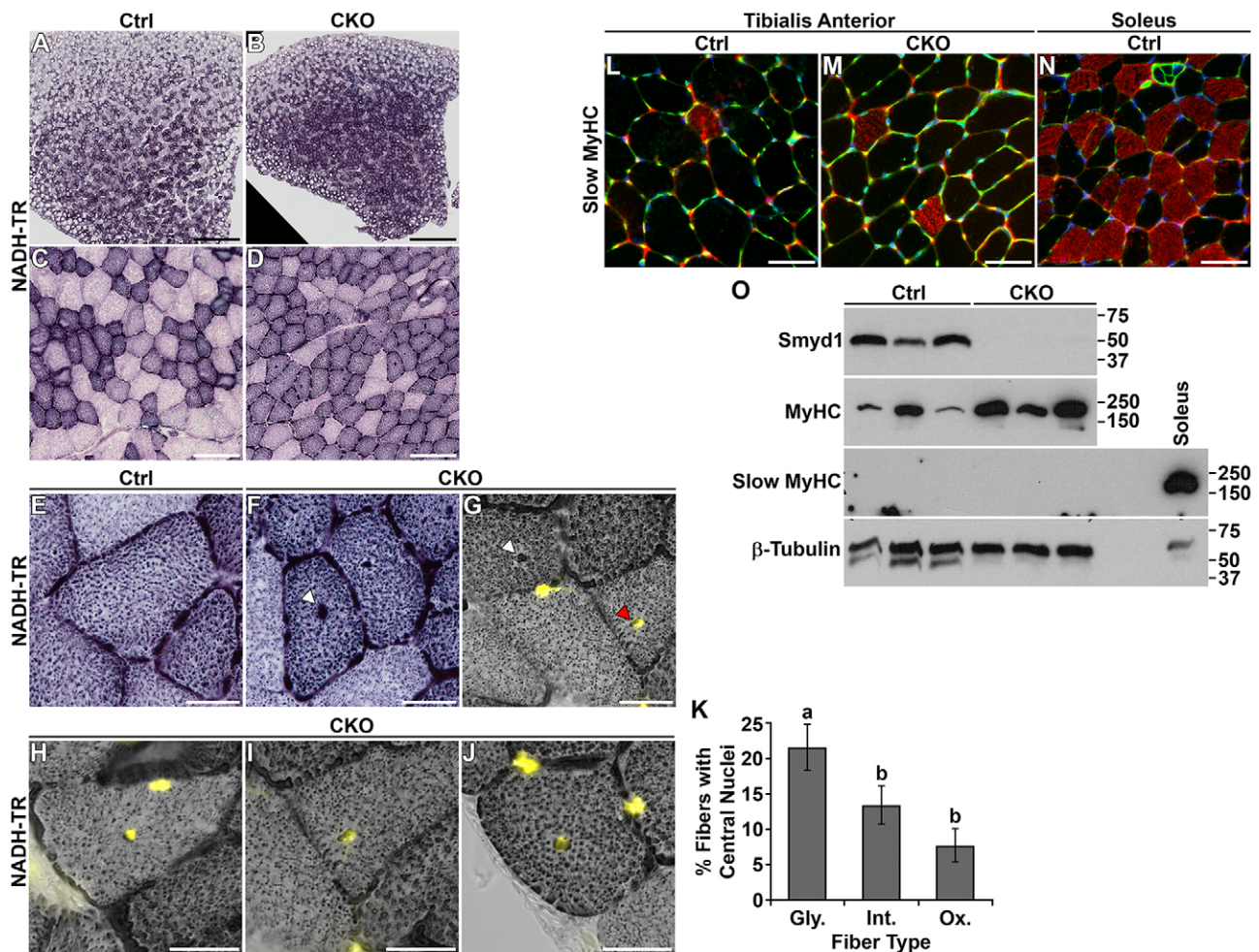


Fig. 5. *Smyd1* CKO mice exhibited increased numbers of oxidative myofibers. (A-J) NADH-TR staining of the tibialis anterior. *Smyd1* CKOs had more fibers with intense oxidative stain (A-D). The only intermyofibrillar network irregularity observed was a central dense focus of oxidative stain (E-G). The dense foci frequently correlated with centralized nuclei [yellow, nuclei (DAPI); white arrowhead, foci of oxidative stain; red arrowhead, foci of oxidative stain that colocalize with a central nucleus] (G). Centralized nuclei were observed in glycolytic (H), intermediate (I) and oxidative (J) fibers. (K) Centralized nuclei were most abundant in glycolytic fibers (CKOs only, $n=5$). Fibers were classified as glycolytic (Gly.), intermediate (Int.) or oxidative (Ox.) based on staining intensity. (L-N) There was no difference in the percentage of type I fibers in the tibialis anterior of control (L) and CKO (M) mice. Soleus was used as a positive control (N). Red, slow MyHC; green, sarcolemma (WGA-488); blue, nuclei (DAPI). (O) Western blots using extracts of tibialis anterior (one animal/lane). SMYD1 protein was undetectable in CKO muscle. Total MyHC increased in the CKO. Slow MyHC was undetectable in both control and CKO tibialis anterior; soleus was included as a positive control. Scale bars: 500 μm (A,B), 100 μm (C,D), 25 μm (E-J) and 50 μm (L-N). All data were obtained from 6-week-old males. Statistics were ANOVA+post-hoc tests. Significant differences ($P<0.05$) are denoted by the lowercase letters above each bar. Error bars show s.e.m. Ctrl, control; CKO, conditional knockout; MyHC, myosin heavy chain.

large number of genes misregulated in these categories (Fig. S9). Very few of these genes encode actual triad components or are direct facilitators of calcium handling in myofibers; therefore, it is unclear whether this represents a meaningful issue with triad function. The results of the RNA-seq were consistent with that obtained by real-time PCR (Table S1). Collectively, our gene expression profiling supports the idea that *Smyd1* CKO myofibers fail to extinguish their developmental gene program or express a low level of regenerative gene activity in response to regional myofibrillar damage.

DISCUSSION

Collectively, our data indicate that myofibers lacking SMYD1 are susceptible to atrophy, weakness, myofibrillar disarray and accumulation of internal nuclei. Broad upregulation of muscle gene expression and internal nuclei in the absence of myofiber regeneration suggests a non-degenerative repair process in response to myofibrillar damage. This phenotype has similarities to human

CNM. CNM comprises a heterogeneous collection of similar diseases, all of which result in a high percentage of myofibers with central nuclei in the absence of degenerating or regenerating myofibers. Because *Smyd1* heterozygous mice are phenotypically normal, myopathies due to *Smyd1* mutations would likely be autosomal recessive. Autosomal recessive CNM has been linked to mutations in the genes encoding the membrane-deforming protein amphiphysin 2 (*BINI*), the major sarcoplasmic reticulum calcium channel ryanodine receptor (*RYR1*) and the giant elastic filament protein titin (*TTN*) (Böhm et al., 2010; Ceyhan-Birsoy et al., 2013; Claeys et al., 2010; Mejaddam et al., 2009; Nicot et al., 2007; Wilmschurst et al., 2010). Similar to *Smyd1* CKO mice, humans with CNM caused by *BINI* mutations often present with hypotrophy, dense oxidative staining in the vicinity of the central nuclei, myofibrillar disorganization and a nonradial sarcoplasmic reticulum pattern. Unlike the *Smyd1* CKO, type I fiber predominance is common (Jungbluth and Gautel, 2014; Nicot et al., 2007; Toussaint

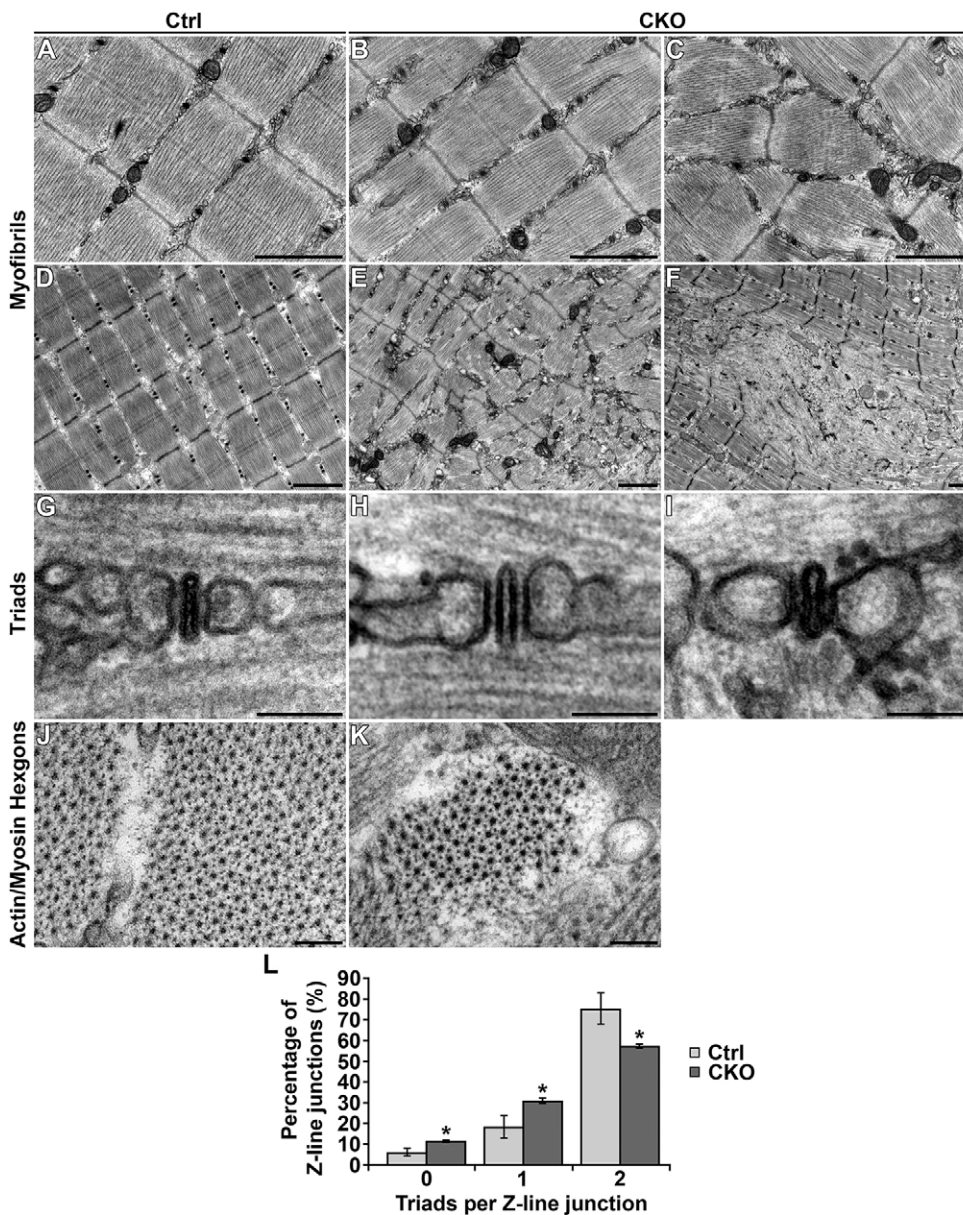


Fig. 6. Abnormal myofibrillar architecture in the absence of SMYD1. (A-K) Ultrastructure images of the tibialis anterior. Control mice exhibited normal myofibrillar architecture (A,D). *Smyd1* CKO muscles showed regions of normal ultrastructure (B), areas of myofibrillar disorganization (C,E) and foci of sarcomere disassembly (F). (G-I) Triads appeared normal regardless of whether they were located in normal regions (H) or regions of disorganization (I). (J,K) *Smyd1* CKO muscles exhibited normal actin/myosin hexagons in transverse sections. (L) *Smyd1* CKO muscle had reduced numbers of triads. Data are the number of Z-lines flanked by zero, one or two triads. *Smyd1* CKO muscles had increased numbers of Z-lines surrounded by zero or one triad and decreased numbers of Z-lines bordered by two triads ($n=3$ animals/group; * $P<0.05$, ANOVA+post-hoc tests). Error bars show s.e.m. Data were obtained from 6-week-old male mice. Scale bars: 1 μm (A-F), 50 nm (G-I) and 100 nm (J,K). Ctrl, control; CKO, conditional knockout.

et al., 2011). Comparable to the *Smyd1* CKO, some individuals with CNM caused by *RYR1* mutations exhibit regional myofibrillar disorganization and hypotrophy (Bevilacqua et al., 2011), but, unlike the *Smyd1* CKO, type I fiber predominance is common (Wilmschurst et al., 2010). Humans with CNM caused by *TTN* mutation present with multiple internal nuclei, type I fiber predominance, hypotrophy and endomysial fibrosis (Ceyhan-Birsoy et al., 2013) – symptoms collectively dissimilar to that observed for the *Smyd1* CKO. The phenotype observed in the *Smyd1* CKO is most similar to a subset of clinical CNM categorized as ‘congenital myopathy with prominent nuclear internalization and large areas of myofibrillar disorganization’ (Romero, 2010). A small subset of individuals with CNM also present with cardiomyopathy. CNM with cardiomyopathy is linked to *SPEG* and *DNM2* mutations, but, in many cases, the genetic cause is unknown (Agrawal et al., 2014; Al-Ruwaishid et al., 2003; Gal et al., 2015; Gospe et al., 1987; Verhies et al., 1976). Because SMYD1 is a crucial regulator of both heart and skeletal muscle development, it is a good candidate for the genetic lesion in cases in

which myofibril disarray presents in both skeletal and cardiac myocytes.

Despite its important functions in striated muscle, *SMYD1* mutations have not been identified in any patient with congenital myopathy. It is known that SMYD1 has a crucial role in heart development (Gottlieb et al., 2002); thus, humans with *SMYD1* mutations would likely exhibit congenital heart defects. No clinical cases of congenital heart defects arising from *SMYD1* mutations have been reported, but one report found single-nucleotide polymorphisms in exon 6 associated with hypertrophic cardiomyopathy (Abaci et al., 2010). Thus, human *SMYD1* loss-of-function mutations might be so detrimental to heart development that, like for mice, embryonic survival is compromised and myopathy is not assessed.

Loss of SMYD1 was more detrimental to males than to females. *Smyd1* CKO males exhibited a greater percent loss of strength, muscle mass and body weight than females. Likewise, CKO females exhibited fewer fibers with central nuclei (19% in males vs 9% in females) and less reduction in myofiber diameter. These

Table 1. Gene expression alterations were specific to fast-twitch muscle

Gene	Tibialis anterior		Soleus	
	Ctrl	CKO	Ctrl	CKO
CNM-related				
<i>Bin1</i>	1.13±0.06	1.62±0.24	1.66±0.13	1.54±0.15
<i>Dnm2</i>	1.42±0.15	2.37±0.46	1.53±0.14	1.74±0.17
<i>Mtm1</i>	1.78±0.22	1.66±0.32	1.60±0.16	1.48±0.17
<i>Mttr14</i>	2.30±0.43	2.12±0.34	1.18±0.11	1.40±0.08
<i>Ptpla</i>	5.14±1.03	↓2.02±0.26**	1.21±0.11	1.27±0.11
<i>Ryr1</i>	1.21±0.12	↑1.98±0.29*	1.62±0.16	1.53±0.11
Myosin isoforms				
<i>Myh1</i>	3.44±0.64	↑10.09±1.82**	2.37±0.23	2.49±0.39
<i>Myh2</i>	3.82±1.42	↑12.27±3.36*	1.44±0.12	1.59±0.15
<i>Myh4</i>	2.25±0.39	↑4.69±0.52**	5.59±2.88	5.21±1.66
<i>Myh7</i>	5.70±2.76	↑84.97±50.19*	1.68±0.28	2.32±0.36
SMYD family				
<i>Smyd2</i>	11.09±0.74	↓3.87±0.32***	1.99±0.17	1.92±0.20
<i>Smyd3</i>	1.81±0.15	2.25±0.24	1.43±0.14	1.66±0.16
<i>Smyd4</i>	2.31±0.22	3.31±0.56	1.52±0.17	1.85±0.17
<i>Smyd5</i>	2.04±0.38	1.96±0.24	1.35±0.11	1.34±0.09

Effect of the *Smyd1* CKO on gene expression in the tibialis anterior and soleus muscles. Real-time PCR was performed using RNA extracted from 6-week-old mice. Values are relative mRNA level \pm s.e.m. Of genes linked to centronuclear myopathy (CNM), expression of *Ptpla* was reduced and *Ryr1* was increased in the tibialis anterior, but not the soleus. Expression of all MyHC isoforms was increased in the tibialis anterior, but not the soleus. Of SMYD family members, expression of *Smyd2* was reduced in the tibialis anterior, but not the soleus. Tibialis anterior, $n=6$ animals/group; soleus, $n\geq 7$ animals/group. * $P<0.05$, ** $P<0.01$, *** $P<0.001$, Student's *t*-test. Ctrl, control; CKO, conditional knockout. Up and down arrows indicate up and downregulation, respectively.

observations suggest that loss of SMYD1-induced myopathy has a greater impact on males than females. Other than in X-linked myotubular myopathy (XLMTM), to our knowledge, the effect of sex on the severity of CNM disease has not been reported. As for prevalence, *DNM2* and *BINI* mutations seem to equally affect both sexes (Böhm et al., 2010; Jeub et al., 2008). *TTN* mutations were only reported in males (Ceyhan-Birsoy et al., 2013). *RYR1* mutations were reported for both males and females (Bevilacqua et al., 2011; Wilmshurst et al., 2010). Our data raise the possibility that gender-specific differences in autosomal CNM have gone unnoticed.

Loss of SMYD1 primarily produced centralized nuclei and hypotrophic fibers in fast-twitch muscles; the soleus was largely unaffected. This fiber-type difference was also apparent in real-time PCR assays where alterations in gene expression were only observed for the tibialis anterior. The pathological differences between fast- and slow-twitch muscles are unlikely to be caused by differences in *Smyd1* expression because approximately equivalent levels of the SMYD1 protein were observed in both tibialis anterior and soleus. Furthermore, SMYD1 exhibited similar sarcomeric localization in both type I and II fibers. Therefore, SMYD1 might have discrete functions in fast- and slow-twitch fibers, and the precise function of SMYD1 in type I fibers remains unknown.

The lack of an obvious phenotype in slow-twitch muscle could be the result of differential expression of a SMYD1 methylation target or SMYD1-interacting molecule. We found no differences in gene expression in control versus *Smyd1* CKO soleus for any of the genes assayed by real-time PCR. Thus, slow-twitch fibers might lack one or more SMYD1-interacting co-regulators or downstream-acting transcription factors. We tested the hypothesis that increased expression of other SMYD family members

compensates for the absence of SMYD1 in the soleus; however, the results of these experiments showed that this was not the case. Expression of *Smyd2*, *3*, *4* and *5* was unaffected in the soleus. In the tibialis anterior, the only SMYD family member with altered expression was *Smyd2* and it was downregulated. SMYD2 contributes to titin stability and maintenance of the I-band by methylating HSP90 (Donlin et al., 2012). Thus, defects in fast-twitch, but not slow-twitch, muscles could be due to a synergistic effect of absence of SMYD1 and reduction of SMYD2.

Smyd1 CKO tibialis anterior exhibited increased numbers of oxidative fibers as assayed by NADH-TR staining. Because there was no increase in abundance of type I fibers in the tibialis anterior, these data most likely reflect an increase in type IIa and IIx fibers. Overexpression of *Myog* promotes switching from glycolytic to oxidative metabolism without altering fiber type (Hughes et al., 1999). Furthermore, *Myog* is expressed to a greater level in oxidative fibers (Voytik et al., 1993). Thus, the increased prevalence of oxidative fibers in the *Smyd1* CKO could explain why *Myog* was upregulated. *Myog* upregulation in this situation might have more to do with increased oxidative metabolism rather than regeneration, which was almost completely absent. Note that, although CKOs exhibited increased numbers of oxidative fibers, central nuclei were most prevalent in glycolytic fibers. Thus, the presence of a central nucleus is not the direct cause of the difference in fiber type, but we cannot exclude the possibility that the oxidative fibers had a central nucleus at some point in the past.

The most striking defect identified by TEM was myofibrillar disorganization. We suspect that the areas of myofibrillar disorder must not be large enough to cause fiber degeneration, but might still promote expression of contractile genes in order to repair the defects. These data support findings in zebrafish, suggesting that SMYD1 is important for sarcomere assembly and stability (Just et al., 2011; Li et al., 2013; Tan et al., 2006). Knockdown of *smyd1a* and *b* in zebrafish embryos severely impairs sarcomerogenesis by 24 hpf, leaving thick and thin filaments in complete disarray. Affected myofibers also exhibited centrally located nuclei. Thus, it was concluded that SMYD1 is required for myofibril organization during myofiber maturation (Tan et al., 2006). Our data are consistent with these observations in that we observed myofibrillar disorganization, albeit not to the extent seen in zebrafish mutants. These differences in phenotype could be due to timing of *Smyd1* ablation. Zebrafish mutants or morphants lose *Smyd1* expression from the myoblast stage, whereas our CKO eliminates *Smyd1* in myofibers perinatally.

The mechanism(s) through which SMYD1 contributes to myofibrillogenesis is largely unknown. SMYD1 colocalizes with nascent myosin in immature sarcomeres and then with the M-line protein myomesin in mature sarcomeres (Just et al., 2011). Thick-filament chaperones *hsp90a1* and *unc45b* are upregulated in zebrafish when *smyd1a/b* expression is reduced (Just et al., 2011; Li et al., 2013). These observations implicate SMYD1 in the regulation of myosin folding, degradation and assembly into sarcomeres. Morpholino-mediated downregulation of zebrafish *smyd1b* led to decreased myosin protein without affecting mRNA levels (Li et al., 2013). In contrast, our data from *Smyd1* CKO mice revealed upregulation of all MyHC isoform genes and concomitant increases in MyHC proteins, with the exception of slow MyHC/Myh7. Because many other muscle developmental genes were upregulated in the *Smyd1* CKO, we suggest that increased expression of MyHC and other muscle genes is a repair response due to myofibril damage or failure to completely mature myofibers.

CNM is considered to be a disease of the triads, the anatomical site of excitation-contraction coupling within a myocyte (Jungbluth and Gautel, 2014). In fact, most of the genes linked to CNM affect the triad either directly or indirectly through importance in membrane curvature or endocytosis. We did not observe structural triad defects, but found reduced numbers of triads in the *Smyd1* CKO tibialis anterior and broad alterations in expression of triad-associated genes. Reduced triad numbers reflect lack of a fully developed triad network, which should envelope each sarcomere. Thus, in *Smyd1* CKO myocytes, there is less triad surface area per sarcomere, which would adversely affect excitation-contraction coupling. Reduced triad numbers might reflect impaired fiber maturation. Alternatively, centrally located nuclei might affect the overall architecture of the intermyofibrillar network. Architectural abnormalities in the intermyofibrillar network could result in decreased numbers of triads per Z-line junction as assayed in this study.

Because SMYD1 is a muscle-specific histone methyltransferase, we suspected that the CKO phenotype would, at least in part, result from altered epigenetic regulation/transcription of genes known to cause CNM. However, reduced mRNA levels were only observed for *Ptpla* (~60% decrease). *Ptpla* (also known as *HACD1*) encodes an enzyme required for elongation of very-long-chain fatty acids (Ikeda et al., 2008), which contributes to the architecture of curved membranes. Triads are structures comprising highly curved membranes and CNM often results from triad defects – thus, establishing a molecular link between *Ptpla* and CNM. Reduced expression of *Ptpla* could impair the construction of triads and lead to reduced triad numbers, as observed in the *Smyd1* CKO.

SMYD1 represses transcription when tethered to DNA, via recruitment of co-repressors to its MYND domain (Gottlieb et al., 2002). Thus, SMYD1 might be a repressor of muscle developmental gene expression. This could explain why SMYD1 is exported from the nucleus to the cytosol during myoblast fusion (Berkholz et al., 2014; Nagandla et al., 2016; Sims et al., 2002) and the reason why muscle development genes were upregulated in the *Smyd1* CKO. The only transcription factor known to interact with SMYD1 is the muscle-specific activator skNAC (Sims et al., 2002; Yotov and St-Arnaud, 1996). Most *skNAC*-null mice die during embryogenesis, owing to heart defects; those that survive exhibit muscle defects, including reduced mass and impaired regeneration, but not CNM (Park et al., 2010). Differences in muscle phenotypes between *skNAC*-null and *Smyd1* CKO mice illustrate non-redundant functions for SMYD1 and skNAC. skNAC is a transcription factor, whereas SMYD1 is both a co-regulator and sarcoplasmic effector of myofibrillogenesis.

In summary, elimination of SMYD1 from skeletal muscle produces a myopathy characterized by increased internal nuclei, hypotrophy, myofibrillar disarray and weakness. Defects primarily manifest within type II fibers, illustrating fiber-type differences in SMYD1's biological activities. Furthermore, our data reveal a gender-specific penetrance in phenotype that could relate to clinical cases where men are more severely affected than women. Collectively, our results suggest that loss of SMYD1 affects myofiber maturation and implicate protein methylation in myofibrillar organization.

MATERIALS AND METHODS

Animals

Smyd1^{lox/lox} mice were developed in collaboration with Dr Haley Tucker (University of Texas, Austin, TX) (Rasmussen et al., 2015). *Smyd1^{+/-}* mice were generated by crossing *Smyd1^{lox/lox}* to the maternal deleter

Tg(Sox2-cre) (Hayashi et al., 2003) (Jackson Laboratory, stock #8454). *Rosa26^{YFP/YFP}* and *Myf6^{cre/+}* mice were obtained from the Jackson Laboratory (stock #7903 and #10528, respectively). Mice for experimental analysis were obtained from the following cross: *Myf6^{cre/+}; Smyd1^{+/-} × Smyd1^{lox/lox}; Rosa26^{YFP/YFP}*. Controls were *Myf6^{cre/+}; Smyd1^{lox/+}; Rosa26^{YFP/+}*. CKOs were *Myf6^{cre/+}; Smyd1^{lox/-}; Rosa26^{YFP/+}*.

The following primers were used for genotyping: Cre-F: 5'-GCCACCA-GCCAGCTATCAACTC-3', Cre-R: 5'-TTGCCCTGTTTCACTATCCAG-3', *Smyd1*-F: 5'-TCATGAGATGGCATGAGCC-3', *Smyd1*-R1 5'-GCA-TACGCACATGTGCTCGC-3', *Smyd1*-R2: 5'-CTCACTTGCGTCCCAGT-ACTTG-3'. *Smyd1*-F/R1 identifies wild-type and flox alleles (432 bp and 552 bp, respectively). *Smyd1*-F/R2 identifies the null allele (~500 bp). All experimental procedures involving mice were approved by the Institutional Animal Care and Use Committee of the University of Houston.

Strength and motor coordination tests

Strength was assayed by a grip strength test. The device consisted of a scale attached to a wire mesh. The scale was immobilized and grip strength was measured by allowing the mouse to grasp the wire mesh with all four paws and then pulling the tail with increasing force until it releases its grip. The test was repeated three times per mouse with a 15 s interval between tests. Data reported is the maximum pull of the three trials.

Strength was also assayed by an inverted grid hang test (Deacon, 2013). This device consists of a wire grid suspended 12 inches above a soft surface. The mouse was placed on the wire grid, which was then inverted such that the mouse was hanging from the grid upside down. Data was time to fall. The trial was stopped if the mouse did not fall after 5 or 8 min for males and females, respectively.

Strength, endurance and motor coordination was assayed by a rotarod test. The test consisted of four trials per day for two consecutive days with 15 min intervals. The rotarod apparatus (Med Associates Inc. ENV-577M) was programmed for continual acceleration from 4 to 40 rpm over 5 min. Data recorded were either the time that had elapsed when the animal fell from the rotarod or when the animal completed two 360° rotations, whichever occurred first.

Body composition

Body composition (% fat and lean mass) was calculated by MRI using an Echo MRI (Echo Medical Systems, Houston, TX).

Evans blue dye uptake

To assay sarcolemmal integrity, one group of mice was not exercised, whereas a second group received a single treadmill exercise regimen of 30 min running at 12 m/min on a 5° incline. Evans blue dye (5 µl of 1% solution in PBS/g body weight) was given by intraperitoneal (IP) injection 30 min post-exercise. The non-exercised group received Evans blue dye at the same time. Tibialis anterior muscle was collected 24 h post-injection as described below. Evans blue dye uptake was assayed in cryosections by far-red fluorescence.

Tissue collection

Muscles were dissected in PBS immediately after euthanasia. Excess PBS was removed by blotting on a paper towel. Muscles were then weighed in pairs using an analytical scale (Denver Instrument, model# SI-114). For RNA or protein extraction, tissues were snap-frozen in liquid nitrogen and stored at -80°C. For histology (H&E staining), tissues were fixed by overnight immersion in Bouin's fluid. For immunofluorescence, Evans blue dye fluorescence and NADH-TR staining, tissues were snap-frozen in liquid-nitrogen-cooled isopentane and stored at -80°C until preparation of cryosections.

Real-time PCR

Total RNA was extracted from muscle using TRIzol reagent according to the manufacturer's protocol (Life Technologies, Carlsbad, CA). mRNA levels were measured using TaqMan gene expression assays with 6-carboxyfluorescein (FAM)-labeled probes from Applied Biosystems (Life Technologies) (Mm00437457_m1 for *Bin1*, Mm00514582_m1 for

Dnm2, Mm01282275_m1 for *Mtm1*, Mm01184733_m1 for *Mtmr14*, Mm01332489_m1 for *Myh1*, Mm01332564_m1 for *Myh2*, Mm01332463_m1 for *Myh3*, Mm01332518_m1 for *Myh4*, Mm01319006_g1 for *Myh7*, Mm01329494_m1 for *Myh8*, Mm01203489_g1 for *Myod1*, Mm00446195_g1 for *Myog*, Mm01354484_m1 for *Pax7*, Mm01729860_m1 for *Ptpla*, Mm01175211_m1 for *Ryr1*, Mm00477663_m1 for *Smyd1*, Mm00660598_m1 for *Smyd2*, Mm00510201_m1 for *Smyd3*, Mm00662052_m1 for *Smyd4* and Mm00523415_m1 for *Smyd5*) and custom oligos for *Pax3* (Pax3-F: 5'-CCAGAGGGCGAAGCTTACC-3', Pax3-R: 5'-GTTGATTGGCTCC-AGCTTGTTT-3', Pax3-Probe: 5'-TCTGGTTTAGCAACCGCCGTG-CA-3', Biosearch Technologies, Petaluma, CA). The level of *Gapdh* mRNA was used for normalization. The PCR was run using an ABI Prism 7900HT thermocycler and SDS2.1 software (Applied Biosystems). Data were analyzed by the comparative $\Delta\Delta CT$ method.

Western blotting

Western blot assays were carried out using total cellular protein. Frozen muscle was homogenized in T-PER buffer (20 ml/g of tissue) (Life Technologies) plus protease and phosphatase inhibitors according to the manufacturer's instructions. Primary antibodies were against Smyd1 (Santa Cruz, cat# sc-79080), myosin heavy chain (MyHC) [Developmental Studies Hybridoma Bank (DSHB), clone MF-20], slow MyHC (DSHB, clone A4.840) or β -tubulin (DSHB, clone E7-c). Membranes were visualized by chemiluminescence using SuperSignal West Pico Chemiluminescent Substrate (Thermo Scientific, Rockford, IL).

Histological analyses

H&E staining was performed using a standard protocol. The percentage of myofibers with centralized nuclei was determined by manual counting. The number of fibers exhibiting centralized (internal) nuclei was divided by the total number of fibers in the tissue cross-section (approximately 2900 fibers/tibialis anterior and 700 fibers/soleus). Myofiber minimum Feret diameter was calculated using the measurement feature of NIS Elements software (Nikon Instruments, Tokyo, Japan). For soleus, 500 fibers were measured. For tibialis anterior, 72 fibers were measured at seven evenly spaced locations (total of 504 fibers).

NADH-TR staining was performed on 10- μ m tibialis anterior cryosections by standard methods. The oxidative reaction was conducted for 15 min at room temperature followed by quenching with PBS. Slides were then stained with DAPI and coverslips mounted with VECTASHIELD HardSet Mounting Medium (Vector Laboratories, Burlingame, CA) to correlate oxidative staining peculiarities with the presence of centralized nuclei.

Immunofluorescence was performed on 10- μ m cryosections by standard methods. 1 \times casein-10% normal serum-PBST was used for protein blocking and as the antibody diluent (10 \times casein stock solution and normal serum were from Vector Laboratories). All slides were stained with DAPI and coverslips mounted with Vectashield Hard Set mounting medium (Vector Laboratories). Antibodies were: goat anti-Smyd1 (Santa Cruz, cat# sc-79080), mouse anti-slow-MyHC (DSHB, clone A4.840) and mouse anti-embryonic-MyHC (DSHB, clone F1.652).

Microscopy

Stereoinages (brightfield and fluorescence) were captured with a Leica MZ10F stereomicroscope and the extended depth-of-focus feature of LAS v3.7 software (Leica Microsystems, Wetzlar, Germany). Brightfield and epifluorescence images of tissue sections were obtained using a Nikon Ti-E inverted microscope equipped with a DS-Fi1 5-megapixel color camera (Nikon Instruments), a CoolSNAP HQ2 14-bit monochrome camera (Photometrics, Tucson, AZ) and NIS Elements software v4.13 (Nikon Instruments).

Transmission electron microscopy

1- to 2- μ m cubes (six cubes/animal) of tibialis anterior muscle were immersion fixed in 0.1 M sodium cacodylate buffer (pH 7.2) containing 2.5% glutaraldehyde and 20 mM calcium chloride. Tissues were post-fixed and heavy-metal-contrasted with potassium ferrocyanide, osmium

tetroxide, thiocarbohydrazide, uranyl acetate and lead aspartate (Lafontant et al., 2013). After dehydration through an acetone series, tissues were embedded in Embed-812 resin (Electron Microscopy Sciences, Hatfield, PA) and ultrathin sections (100 nm) were imaged on a Tecnai G2 Spirit BioTWIN (FEI Company, Hillsboro, OR) electron microscope. The abundance of triads was calculated by counting the number of triads per Z-line junction. At least 75 non-overlapping images were captured per animal at 26,500 \times from at least 15 individual fibers. Images were evenly spaced along the length of each fiber and no more than five images were captured per fiber.

RNA-seq

Tibialis anterior total RNA (100 ng) from six control and six CKO mice was depleted of ribosomal RNA using the ScriptSeq Complete Gold kit from Epicentre (cat# SCL24EP) following the manufacturer's instructions. The 12 libraries were submitted at a 20 nM-multiplexed concentration for sequencing on the Illumina HiSeq platform at the DNA core facility at the University of Texas M. D. Anderson Cancer Center (Houston, TX). After adapters were trimmed from raw RNA-seq data, reads were aligned to the mouse genome using bowtie2 (Langmead et al., 2009) and tophat (Trapnell et al., 2009), allowing at most two mismatches. Reads that mapped to multiple locations in the genome were discarded. The abundance of each transcript was computed using cufflinks. The abundance of each transcript was expressed as FPKM (fragments per kilobase of transcript per million mapped reads). We used DESeq to obtain differentially expressed ($P < 0.05$) genes between two conditions (Anders and Huber, 2010). Genes with less than three aligned read counts across all the samples were not considered. Enriched gene ontology terms were obtained using DAVID (Huang et al., 2009) with the mouse genome as the background set of genes. Robust z -score, which was computed for each gene from the FPKM values across all the replicates of the two conditions, was used to generate the heat maps. The dataset was deposited to the NCBI Gene Expression Omnibus (GEO) database under series accession number GSE71679 (<http://www.ncbi.nlm.nih.gov/geo/query/acc.cgi?acc=GSE71679>).

Statistical analyses

For experiments with more than two experimental groups, quantitative data were subjected to one-way analysis of variance (ANOVA) using MedCalc v14.12.0 software (MedCalc Software bvba, Belgium). Rotarod data was analyzed by two-way ANOVA. If the ANOVA was positive ($P < 0.05$), a post-hoc Student–Newman–Keuls test was performed for pairwise comparison of subgroups. For studies with two experimental groups, an independent samples Student's t -test was performed. A P -value of < 0.05 was considered significant for all tests.

Acknowledgements

The authors thank Dr Tom Lowder (University of Houston) for assistance with MRI and Dr MariVi Tejada-Simon (University of Houston) for help with rotarod tests. We thank Evelyn Brown and Margaret Gondo for excellent technical assistance in preparing and imaging tissue samples for electron microscopy. The slow and embryonic MyHC monoclonal antibodies used in this study were developed by H. M. Blau and were obtained from the Developmental Studies Hybridoma Bank, created by the NICHD of the NIH and maintained at The University of Iowa.

Competing interests

The authors declare no competing or financial interests.

Author contributions

M.D.S. and R.J.S. designed the research; M.D.S., S.L., H.N., A.B., J.N., N.V. and H.J.W. performed the research; T.L.R. and H.O.T. contributed new reagents/analytical tools; M.D.S., B.S. and A.R.B. analyzed data; and M.D.S. and H.O.T. wrote the paper.

Funding

This work was supported by the American Heart Association [12BGIA11860006 to M.D.S.]; the University of Houston Division of Research Small Grants Program [1HOU08 to M.D.S.]; the Texas Heart Institute [M.D.S. and R.J.S.]; the National Institutes of Health/National Eye Institute (NIH/NEI) [P30EY007551 to A.R.B.]; and the Cancer Prevention and Research Institute of Texas (CPRIT) [RP120348 and RP120459 to H.O.T.].

Supplementary information

Supplementary information available online at
<http://dmm.biologists.org/lookup/suppl/doi:10.1242/dmm.022491/-/DC1>

References

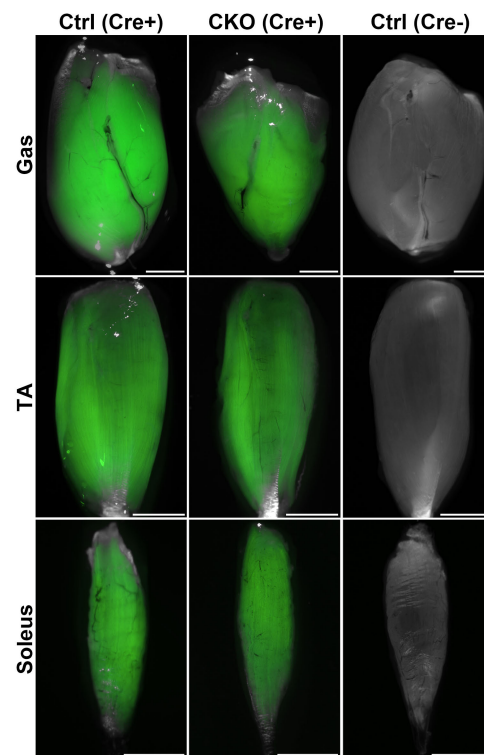
- Abaci, N., Gulec, C., Bayrak, F., Komurcu Bayrak, E., Kahveci, G. and Erginel Unaltuna, N. (2010). The variations of BOP gene in hypertrophic cardiomyopathy. *Anadolu Kardiyol. Derg.* **10**, 303-309.
- Agrawal, P. B., Pierson, C. R., Joshi, M., Liu, X., Ravenscroft, G., Moghadaszadeh, B., Talabere, T., Viola, M., Swanson, L. C., Haliloğlu, G. et al. (2014). SPEG interacts with myotubularin, and its deficiency causes centronuclear myopathy with dilated cardiomyopathy. *Am. J. Hum. Genet.* **95**, 218-226.
- Al-Ruwaisid, A., Vajsar, J., Tein, I., Benson, L. and Jay, V. (2003). Centronuclear myopathy and cardiomyopathy requiring heart transplant. *Brain Dev.* **25**, 62-66.
- Anders, S. and Huber, W. (2010). Differential expression analysis for sequence count data. *Genome Biol.* **11**, R106.
- Berkholz, J., Michalick, L. and Munz, B. (2014). The E3 SUMO ligase Nse2 regulates sumoylation and nuclear-to-cytoplasmic translocation of skNAC-Smyd1 in myogenesis. *J. Cell Sci.* **127**, 3794-3804.
- Bevilacqua, J. A., Monnier, N., Bitoun, M., Eymard, B., Ferreira, A., Monges, S., Lubieniecki, F., Taratuto, A. L., Laquerrière, A., Claeys, K. G. et al. (2011). Recessive RYR1 mutations cause unusual congenital myopathy with prominent nuclear internalization and large areas of myofibrillar disorganization. *Neuropathol. Appl. Neurobiol.* **37**, 271-284.
- Böhm, J., Yiş, U., Ortaç, R., Çakmakçı, H., Kurul, S. H., Dirik, E. and Laporte, J. (2010). Case report of intrafamilial variability in autosomal recessive centronuclear myopathy associated to a novel BIN1 stop mutation. *Orphanet J. Rare Dis.* **5**, 35.
- Bohm, J., Biancalana, V., Malfatti, E., Dondaine, N., Koch, C., Vasli, N., Kress, W., Strittmatter, M., Taratuto, A. L., Gonorazky, H. et al. (2014). Adult-onset autosomal dominant centronuclear myopathy due to BIN1 mutations. *Brain* **137**, 3160-3170.
- Ceyhan-Birsoy, O., Agrawal, P. B., Hidalgo, C., Schmitz-Abe, K., DeChene, E. T., Swanson, L. C., Soemedi, R., Vasli, N., Iannaccone, S. T., Shieh, P. B. et al. (2013). Recessive truncating titin gene, TTN, mutations presenting as centronuclear myopathy. *Neurology* **81**, 1205-1214.
- Chen, T., Pu, C., Wang, Q., Liu, J., Mao, Y. and Shi, Q. (2015). Clinical, pathological, and genetic features of dynamin-2-related centronuclear myopathy in China. *Neurol. Sci.* **36**, 735-741.
- Claeys, K. G., Maisonobe, T., Bohm, J., Laporte, J., Hezode, M., Romero, N. B., Brochier, G., Bitoun, M., Carlier, R. Y. and Stojkovic, T. (2010). Phenotype of a patient with recessive centronuclear myopathy and a novel BIN1 mutation. *Neurology* **74**, 519-521.
- Cowling, B. S., Chevremont, T., Prokic, I., Kretz, C., Ferry, A., Coirault, C., Koutsopoulos, O., Laugel, V., Romero, N. B. and Laporte, J. (2014). Reducing dynamin 2 expression rescues X-linked centronuclear myopathy. *J. Clin. Invest.* **124**, 1350-1363.
- Deacon, R. M. (2013). Measuring the strength of mice. *J. Vis. Exp.*
- Donlin, L. T., Andresen, C., Just, S., Rudensky, E., Pappas, C. T., Kruger, M., Jacobs, E. Y., Unger, A., Zieseniss, A., Dobenecker, M.-W. et al. (2012). Smyd2 controls cytoplasmic lysine methylation of Hsp90 and myofilament organization. *Genes Dev.* **26**, 114-119.
- Gal, A., Inczedy-Farkas, G., Pal, E., Remenyi, V., Bereznai, B., Geller, L., Széldi, Z., Merkely, B. and Molnar, M. J. (2015). The coexistence of dynamin 2 mutation and multiple mitochondrial DNA (mtDNA) deletions in the background of severe cardiomyopathy and centronuclear myopathy. *Clin. Neuropathol.* **34**, 89-95.
- Gao, J., Li, J., Li, B.-J., Yagil, E., Zhang, J. and Du, S. J. (2014). Expression and functional characterization of Smyd1a in myofibril organization of skeletal muscles. *PLoS ONE* **9**, e86808.
- Gospe, S. M., Jr, Armstrong, D. L., Gresik, M. V. and Hawkins, H. K. (1987). Life-threatening congestive heart failure as the presentation of centronuclear myopathy. *Pediatr. Neurol.* **3**, 117-120.
- Gottlieb, P. D., Pierce, S. A., Sims, R. J., Yamagishi, H., Weihe, E. K., Harriss, J. V., Maika, S. D., Kuziel, W. A., King, H. L., Olson, E. N. et al. (2002). Bop encodes a muscle-restricted protein containing MYND and SET domains and is essential for cardiac differentiation and morphogenesis. *Nat. Genet.* **31**, 25-32.
- Hayashi, S., Tenzen, T. and McMahon, A. P. (2003). Maternal inheritance of Cre activity in a Sox2Cre deleter strain. *Genesis* **37**, 51-53.
- Huang, D. W., Sherman, B. T. and Lempicki, R. A. (2009). Bioinformatics enrichment tools: paths toward the comprehensive functional analysis of large gene lists. *Nucleic Acids Res.* **37**, 1-13.
- Hughes, S. M., Chi, M. M., Lowry, O. H. and Gundersen, K. (1999). Myogenin induces a shift of enzyme activity from glycolytic to oxidative metabolism in muscles of transgenic mice. *J. Cell Biol.* **145**, 633-642.
- Hwang, I. and Gottlieb, P. D. (1997). The Bop gene adjacent to the mouse CD8b gene encodes distinct zinc-finger proteins expressed in CTLs and in muscle. *J. Immunol.* **158**, 1165-1174.
- Ikeda, M., Kanao, Y., Yamanaka, M., Sakuraba, H., Mizutani, Y., Igarashi, Y. and Kihara, A. (2008). Characterization of four mammalian 3-hydroxyacyl-CoA dehydratases involved in very long-chain fatty acid synthesis. *FEBS Lett.* **582**, 2435-2440.
- Jeub, M., Bitoun, M., Guicheney, P., Kappes-Horn, K., Strach, K., Druschky, K. F., Weis, J. and Fischer, D. (2008). Dynamin 2-related centronuclear myopathy: clinical, histological and genetic aspects of further patients and review of the literature. *Clin. Neuropathol.* **27**, 430-438.
- Jungbluth, H. and Gautel, M. (2014). Pathogenic mechanisms in centronuclear myopathies. *Front. Aging Neurosci.* **6**, 339.
- Just, S., Meder, B., Berger, I. M., Etard, C., Trano, N., Patzel, E., Hassel, D., Marquart, S., Dahme, T., Vogel, B. et al. (2011). The myosin-interacting protein SMYD1 is essential for sarcomere organization. *J. Cell Sci.* **124**, 3127-3136.
- Kawamura, S., Yoshigai, E., Kuhara, S. and Tashiro, K. (2008). smyd1 and smyd2 are expressed in muscle tissue in *Xenopus laevis*. *Cytotechnology* **57**, 161-168.
- Keller, C., Arenkiel, B. R., Coffin, C. M., El-Bardeesy, N., DePinho, R. A. and Capecchi, M. R. (2004). Alveolar rhabdomyosarcomas in conditional Pax3:Fkhr mice: cooperativity of Ink4a/ARF and Trp53 loss of function. *Genes Dev.* **18**, 2614-2626.
- Lafontant, P. J., Behzad, A. R., Brown, E., Landry, P., Hu, N. and Burns, A. R. (2013). Cardiac myocyte diversity and a fibroblast network in the junctional region of the zebrafish heart revealed by transmission and serial block-face scanning electron microscopy. *PLoS ONE* **8**, e72388.
- Langmead, B., Trapnell, C., Pop, M. and Salzberg, S. L. (2009). Ultrafast and memory-efficient alignment of short DNA sequences to the human genome. *Genome Biol.* **10**, R25.
- Li, D., Niu, Z., Yu, W., Qian, Y., Wang, Q., Li, Q., Yi, Z., Luo, J., Wu, X., Wang, Y. et al. (2009). SMYD1, the myogenic activator, is a direct target of serum response factor and myogenin. *Nucleic Acids Res.* **37**, 7059-7071.
- Li, H., Xu, J., Bian, Y.-H., Rotllant, P., Shen, T., Chu, W., Zhang, J., Schneider, M. and Du, S. J. (2011). Smyd1b_tv1, a key regulator of sarcomere assembly, is localized on the M-line of skeletal muscle fibers. *PLoS ONE* **6**, e28524.
- Li, H., Zhong, Y., Wang, Z., Gao, J., Xu, J., Chu, W., Zhang, J., Fang, S. and Du, S. J. (2013). Smyd1b is required for skeletal and cardiac muscle function in zebrafish. *Mol. Biol. Cell* **24**, 3511-3521.
- Liu, Y., Chen, W., Gaudet, J., Cheney, M. D., Roudaia, L., Cierpicki, T., Klet, R. C., Hartman, K., Laue, T. M., Speck, N. A. et al. (2007). Structural basis for recognition of SMRT/N-CoR by the MYND domain and its contribution to AML1/ETO's activity. *Cancer Cell* **11**, 483-497.
- Lutterbach, B., Sun, D., Schuetz, J. and Hiebert, S. W. (1998). The MYND motif is required for repression of basal transcription from the multidrug resistance 1 promoter by the t(8;21) fusion protein. *Mol. Cell Biol.* **18**, 3604-3611.
- Masselink, H. and Bernards, R. (2000). The adenovirus E1A binding protein BS69 is a corepressor of transcription through recruitment of N-CoR. *Oncogene* **19**, 1538-1546.
- Mejaddam, A. Y., Nennesmo, I. and Sejersen, T. (2009). Severe phenotype of a patient with autosomal recessive centronuclear myopathy due to a BIN1 mutation. *Acta Myol.* **28**, 91-93.
- Nagandla, H., Lopez, S., Yu, W., Rasmussen, T. L., Tucker, H. O., Schwartz, R. J. and Stewart, M. D. (2016). Defective myogenesis in the absence of the muscle-specific lysine methyltransferase SMYD1. *Dev. Biol.* **410**, 86-97.
- Nicot, A.-S., Toussaint, A., Tosch, V., Kretz, C., Wallgren-Pettersson, C., Iwarsson, E., Kingston, H., Garnier, J.-M., Biancalana, V., Oldfors, A. et al. (2007). Mutations in amphiphysin 2 (BIN1) disrupt interaction with dynamin 2 and cause autosomal recessive centronuclear myopathy. *Nat. Genet.* **39**, 1134-1139.
- Park, C. Y., Pierce, S. A., von Drehle, M., Ivey, K. N., Morgan, J. A., Blau, H. M. and Srivastava, D. (2010). skNAC, a Smyd1-interacting transcription factor, is involved in cardiac development and skeletal muscle growth and regeneration. *Proc. Natl. Acad. Sci. USA* **107**, 20750-20755.
- Rasmussen, T. L., Ma, Y., Park, C. Y., Harriss, J., Pierce, S. A., Dekker, J. D., Valenzuela, N., Srivastava, D., Schwartz, R. J., Stewart, M. D. et al. (2015). Smyd1 facilitates heart development by antagonizing oxidative and ER stress responses. *PLoS ONE* **10**, e0121765.
- Romero, N. B. (2010). Centronuclear myopathies: a widening concept. *Neuromuscul. Disord.* **20**, 223-228.
- Romero, N. B. and Bitoun, M. (2011). Centronuclear myopathies. *Semin. Pediatr. Neurol.* **18**, 250-256.
- Sims, R. J., III, Weihe, E. K., Zhu, L., O'Malley, S., Harriss, J. V. and Gottlieb, P. D. (2002). m-Bop, a repressor protein essential for cardiogenesis, interacts with skNAC, a heart- and muscle-specific transcription factor. *J. Biol. Chem.* **277**, 26524-26529.
- Sirinpong, N., Brunzelle, J., Ye, J., Pirzada, A., Nico, L. and Yang, Z. (2010). Crystal structure of cardiac-specific histone methyltransferase Smyd1 reveals unusual active site architecture. *J. Biol. Chem.* **285**, 40635-40644.

- Strahl, B. D., Ohba, R., Cook, R. G. and Allis, C. D.** (1999). Methylation of histone H3 at lysine 4 is highly conserved and correlates with transcriptionally active nuclei in *Tetrahymena*. *Proc. Natl. Acad. Sci. USA* **96**, 14967-14972.
- Tan, X., Rotllant, J., Li, H., De Deyne, P. and Du, S. J.** (2006). SmyD1, a histone methyltransferase, is required for myofibril organization and muscle contraction in zebrafish embryos. *Proc. Natl. Acad. Sci. USA* **103**, 2713-2718.
- Toussaint, A., Cowling, B. S., Hnia, K., Mohr, M., Oldfors, A., Schwab, Y., Yis, U., Maisonobe, T., Stojkovic, T., Wallgren-Pettersson, C. et al.** (2011). Defects in amphiphysin 2 (BIN1) and triads in several forms of centronuclear myopathies. *Acta Neuropathol.* **121**, 253-266.
- Trapnell, C., Pachter, L. and Salzberg, S. L.** (2009). TopHat: discovering splice junctions with RNA-Seq. *Bioinformatics* **25**, 1105-1111.
- Verhies, W., Brucher, J. M., Goddeeris, P., Lauweryns, J. and De Geest, H.** (1976). Familial centronuclear myopathy associated with 'cardiomyopathy'. *Br. Heart J.* **38**, 504-509.
- Voytik, S. L., Przyborski, M., Badylak, S. F. and Konieczny, S. F.** (1993). Differential expression of muscle regulatory factor genes in normal and denervated adult rat hindlimb muscles. *Dev. Dyn.* **198**, 214-224.
- Wilmshurst, J. M., Lillis, S., Zhou, H., Pillay, K., Henderson, H., Kress, W., Müller, C. R., Ndong, A., Cloke, V., Cullup, T. et al.** (2010). RYR1 mutations are a common cause of congenital myopathies with central nuclei. *Ann. Neurol.* **68**, 717-726.
- Yotov, W. V. and St-Arnaud, R.** (1996). Differential splicing-in of a proline-rich exon converts alphaNAC into a muscle-specific transcription factor. *Genes Dev.* **10**, 1763-1772.

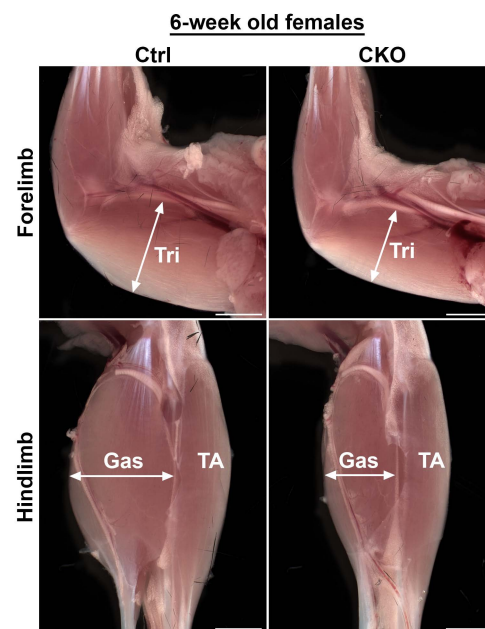
Suppl. Table S1. Good correlation between gene expression data obtained by RNA-seq and real-time PCR.

Gene	RNA-seq	Real-Time PCR
<u>Regeneration</u>		
<i>Pax3</i>	NS	NS
<i>Pax7</i>	↑ 1.76	↑ 1.58
<i>Myod1</i>	NS	NS
<i>Myog</i>	↑ 2.54	↑ 2.44
<i>Myh3</i>	↑ 11.07	↑ 12.88
<i>Myh8</i>	NS	NS
<u>CNM-Associated</u>		
<i>Bin1</i>	NS	NS
<i>Dnm2</i>	NS	NS
<i>Mtm1</i>	NS	NS
<i>Mtmr14</i>	NS	NS
<i>Ptpla</i>	↓ 0.82	↓ 0.39
* <i>Ryr1</i>	NS	↑ 1.63
<u>MyHC Isoforms</u>		
<i>Myh1</i>	↑ 2.14	↑ 2.94
<i>Myh2</i>	↑ 2.39	↑ 3.21
<i>Myh4</i>	↑ 1.74	↑ 2.08
<i>Myh7</i>	↑ 13.64	↑ 14.91
<u>Smyd Family</u>		
<i>Smyd2</i>	↓ 0.39	↓ 0.35
<i>Smyd3</i>	NS	NS
<i>Smyd4</i>	NS	NS
<i>Smyd5</i>	NS	NS

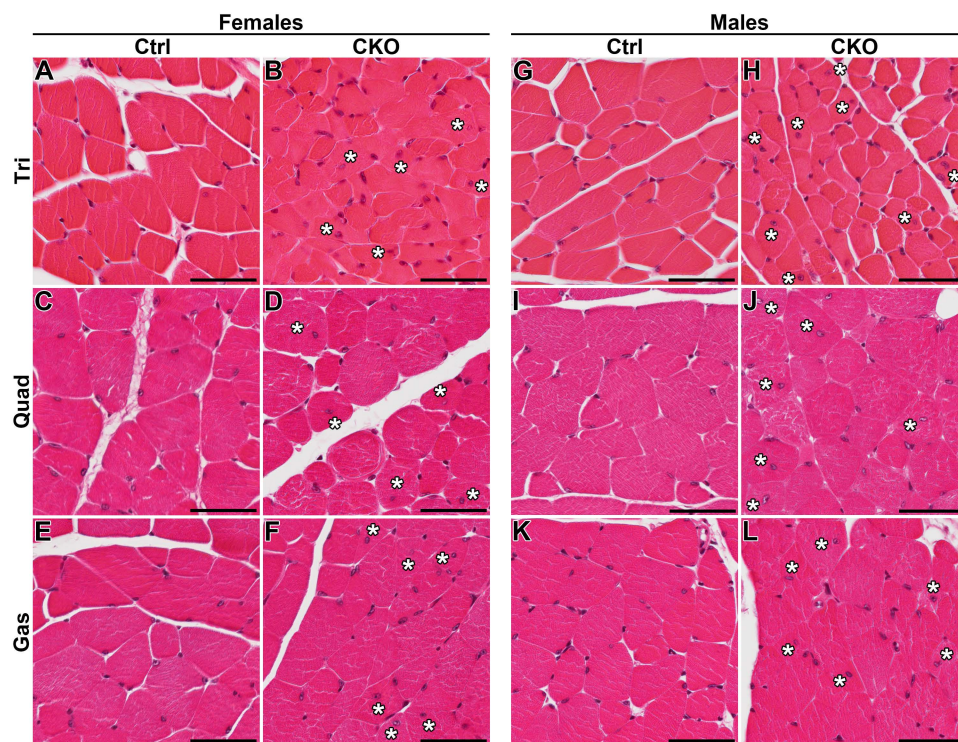
Right column is a summary of all real-time PCR gene expression assays reported in this manuscript. Center column contains the RNA-seq results for those same genes. Tissues were tibialis anterior. Values reported are fold change (*Smyd1* CKO/Control). Up and down arrows indicate upregulation and downregulation, respectively. Values reported if $P < 0.05$. *Only for *Ryr1* did RNA-seq and real-time PCR data not correlate. NS, difference was not significant.



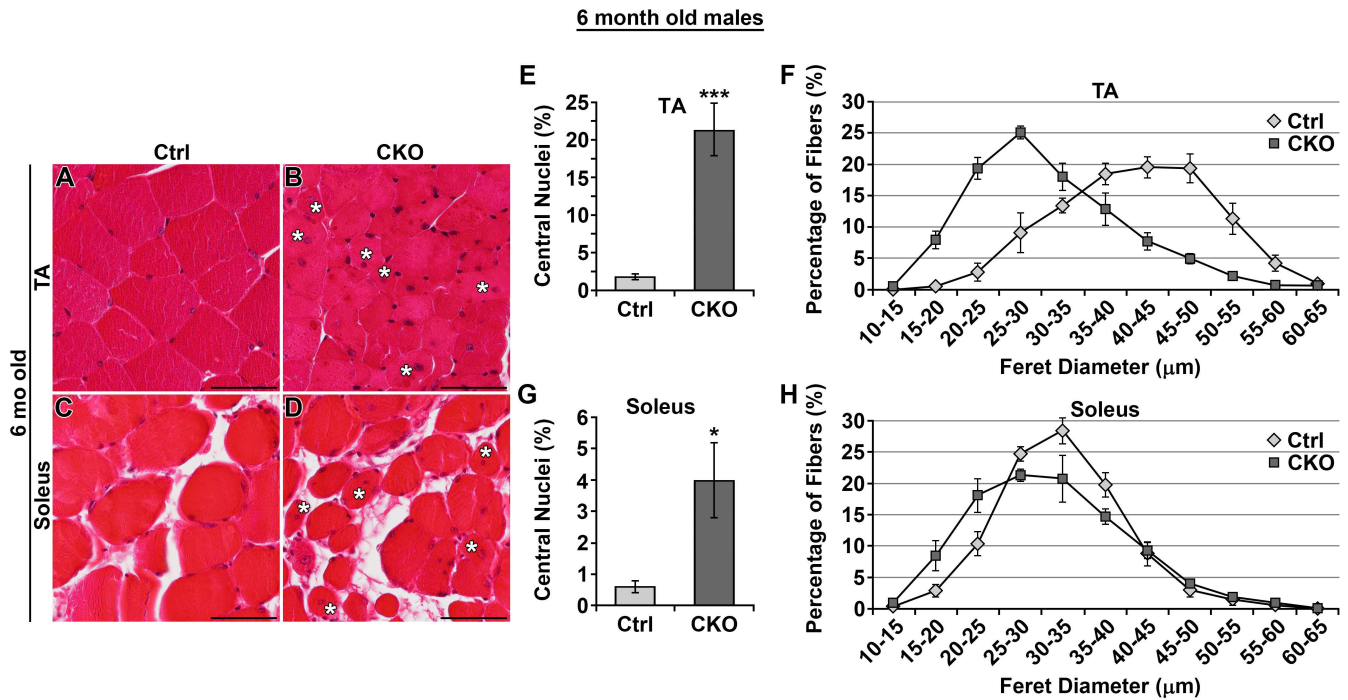
Suppl. Fig. S1. *Myf6^{cre}* induces recombination of *loxP* sites in skeletal muscles. Our genetic approach included the *Rosa26^{YFP}* allele (*Myf6^{cre/+}*; *Smyd1^{+/-}* x *Smyd1^{fllox/fllox}*; *Rosa26^{YFP/YFP}*), which allowed us to monitor cells derived from *Myf6^{cre}*-expressing cells. We confirmed that *Myf6^{cre}* induces recombination of *loxP* sites in all muscles examined by imaging YFP fluorescence under a stereofluorescence microscope. Muscles from *Myf6^{+/+}*; *Smyd1^{fllox/-}*; *Rosa26^{YFP/+}* animals [Ctrl (Cre-)], which should not express YFP, were used as a negative control (rightmost column). Scale bars are 2 mm. Ctrl, control; CKO, conditional knockout; Gas, gastrocnemius; TA, tibialis anterior.



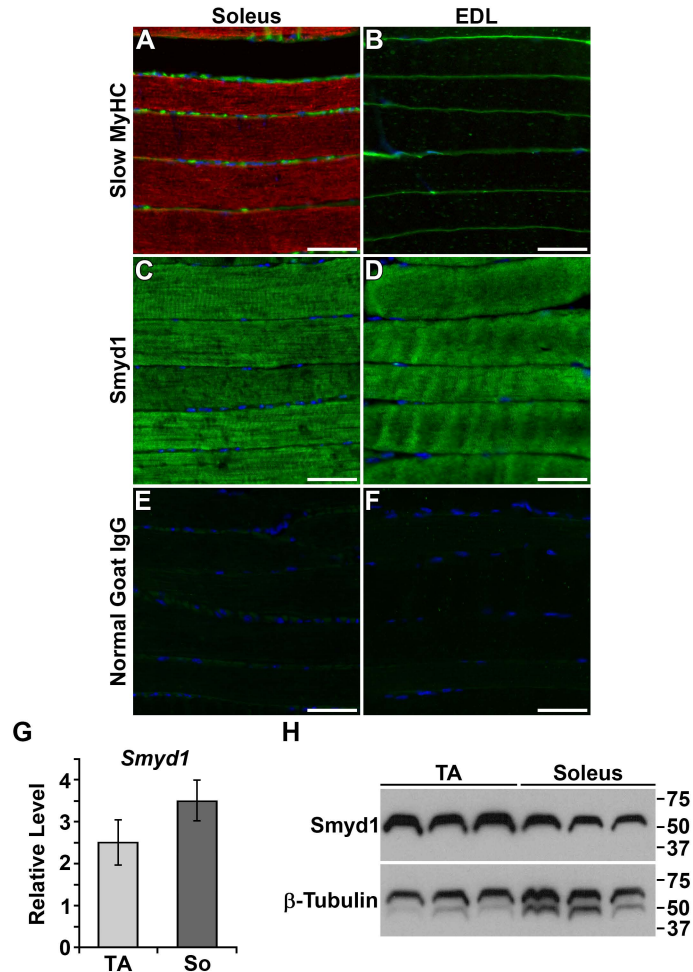
Suppl. Fig. S2. Reduced muscle mass in *Smyd1* CKO females. Stereomicrographs of the muscles of the forelimbs and hindlimbs of female control and *Smyd1* CKO mice at 6 weeks of age. Scale bars are 2 mm. Ctrl, control; CKO, conditional knockout; Gas, gastrocnemius; TA, tibialis anterior; Tri, triceps.



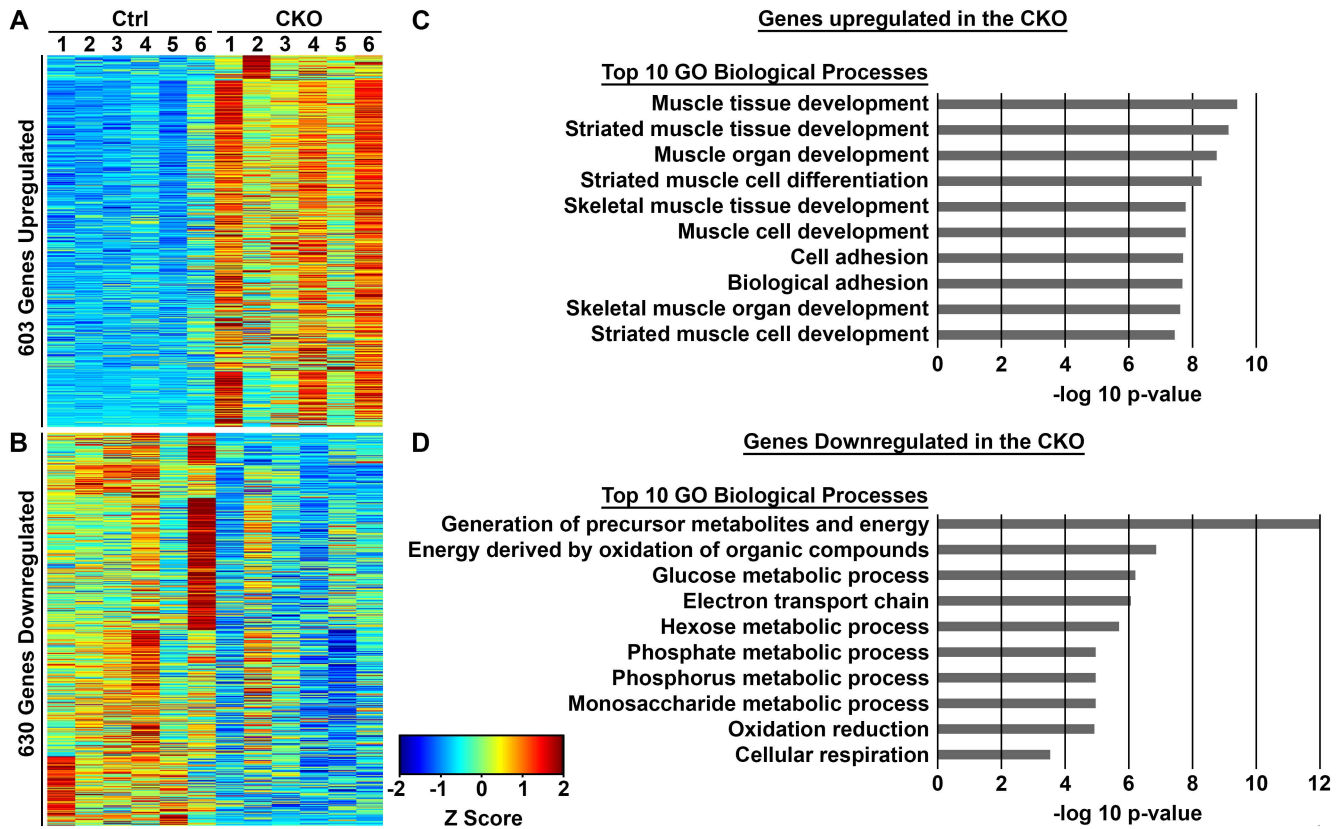
Suppl. Fig. S3. High prevalence of fibers with central nuclei in triceps, quadriceps and gastrocnemius. Images of H&E-stained muscle sections from 6-week old female (A-F) and male (G-L) mice. Very few fibers with central nuclei were observed in the muscles of control mice (A, C, E, G, I and K). Central nuclei were prevalent in male and female *Smyd1* CKO triceps (B and H), quadriceps (D and J) and gastrocnemius (F and L). White asterisks (*) indicate fibers with central nuclei. Scale bars are 50 μm . Ctrl, control; CKO, conditional knockout; Gas, gastrocnemius; Tri, triceps; Quad, quadriceps.



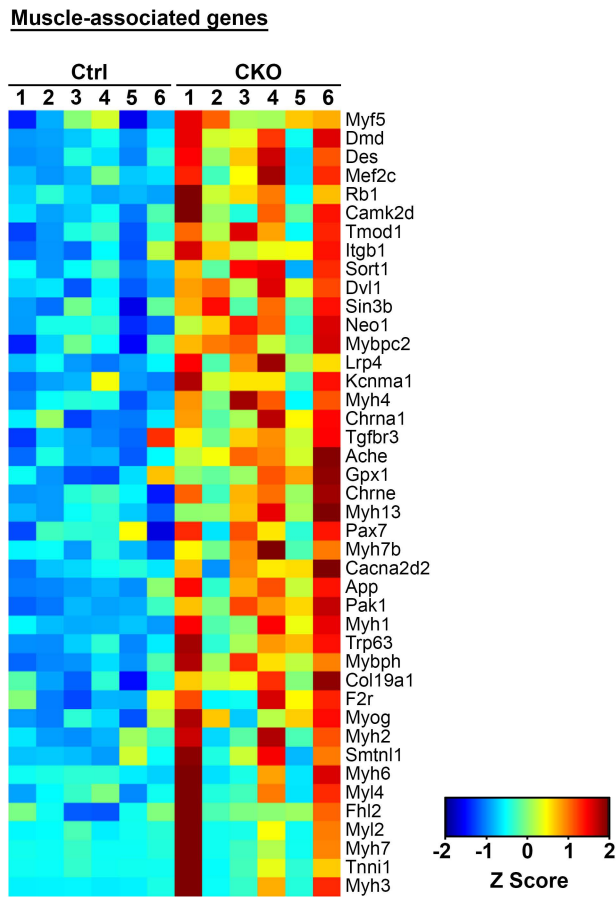
Suppl. Fig. S4. Slight disease progression by 6 months of age. (A-D) Images of H&E-stained muscle sections from 6-month old mice. White asterisks (*) indicate central nuclei. Central nuclei were prevalent in *Smyd1* CKO muscles. (E) Quantification of the percentage of myofibers in the tibialis anterior with central nuclei ($n \geq 3$ animals/group). (F) Distribution of myofiber minimum Feret diameter in the tibialis anterior. *Smyd1* CKO tibialis anterior had increased numbers of hypotrophic fibers ($P = 0.0018$, $n \geq 3$ animals/group). (G) Quantification of the percentage of myofibers in the soleus with central nuclei ($n \geq 6$ animals/group). (H) Distribution of myofiber minimum Feret diameter in the soleus. Mean myofiber minimum Feret diameter was not significantly different for the soleus ($n \geq 3$ animals/group). * $P < 0.05$, *** $P < 0.001$, Student's t test. Error bars show SEM. Scale bars are 50 μm . Ctrl, control; CKO, conditional knockout; TA, tibialis anterior.



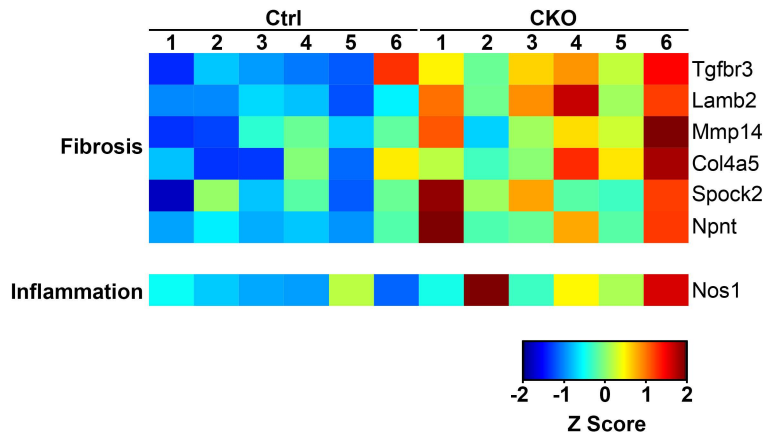
Suppl. Fig. S5. *Smyd1* is expressed in all fiber types. (A-F) Immunolocalization of slow MyHC (red) (A, B) and Smyd1 (green) (C, D) in the EDL and soleus. Normal goat IgG was used as a negative control (E, F). For A and B, sarcolemmas are labeled with WGA-488 (green). Smyd1 protein was detectable in all fibers. Scale bars are 50 μ m. (G) Real-time PCR assay. The *Smyd1* gene is expressed to equivalent levels in the tibialis anterior and soleus ($n = 6$ animals/group). (H) Western blot to compare SMYD1 protein levels in tibialis anterior and soleus. Each lane contains protein extract from an individual animal. SMYD1 protein levels appeared to be slightly lower in the soleus. Anti- β -tubulin was used as a loading control. Molecular weight (kDa) is indicated to the right of each blot.



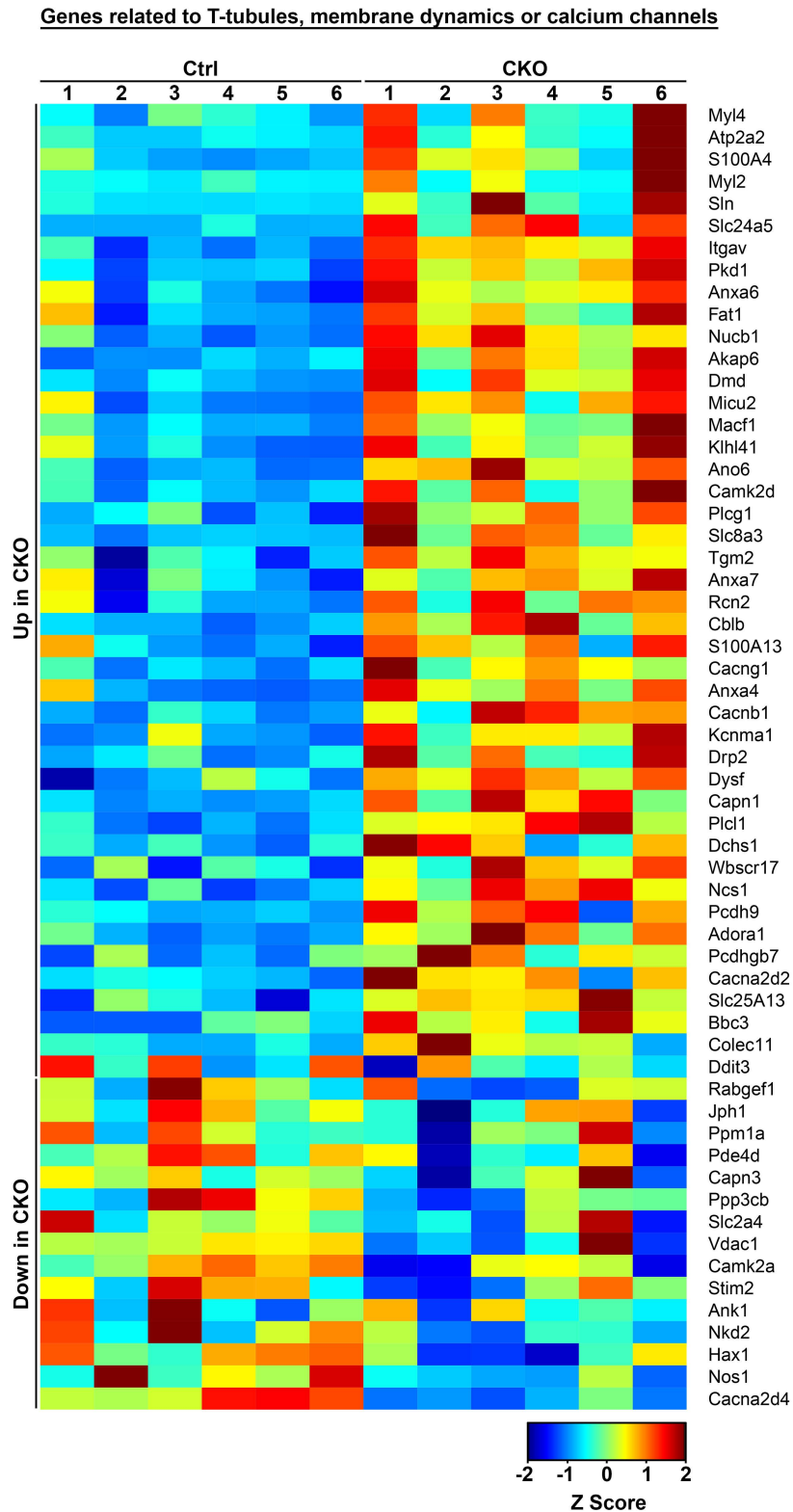
Suppl. Fig. S6. Genes involved in muscle development are upregulated in *Smyd1* CKO muscle. Results of RNA-seq analysis. (A and B) Heat maps of all genes upregulated (A) or downregulated (B) in the *Smyd1* CKO (cutoff was $P < 0.05$). (C and D) Top 10 biological processes gene ontology terms associated with those genes upregulated (C) or downregulated (D) in the *Smyd1* CKO tibialis anterior. Tissues (tibialis anterior) were collected from 6-week old mice. $n = 6$ animals/group. Ctrl, control; CKO, conditional knockout; GO, gene ontology.



Suppl. Fig. S7. Heat map of muscle-associated genes upregulated in the *Smyd1* CKO. Each column contains RNA-seq results from a single animal. Tissues (tibialis anterior) were collected from 6-week old mice ($n = 6$ /group). Ctrl, control; CKO, conditional knockout.



Suppl. Fig. S8. Very few genes associated with fibrosis or inflammation showed altered expression in the *Smyd1* CKO. Each column contains RNA-seq results from a single animal. Tissues (tibialis anterior) were collected from 6-week old mice ($n = 6$ /group). Ctrl, control; CKO, conditional knockout.



Suppl. Fig. S9. Altered expression of genes related to T-tubules, membrane dynamics or calcium channels in the *Smyd1* CKO. Each column contains RNA-seq results from a single animal. Tissues (tibialis anterior) were collected from 6-week old mice ($n = 6/\text{group}$). Ctrl, control; CKO, conditional knockout.